

NON-EUCLIDEAN GRADIENT DESCENT OPERATES AT THE EDGE OF STABILITY

005 **Anonymous authors**

006 Paper under double-blind review

ABSTRACT

011 The Edge of Stability (EoS) is a phenomenon where the sharpness (largest eigen-
 012 value) of the Hessian converges to $2/\eta$ during training with gradient descent (GD)
 013 with a step-size η . Despite violating classical smoothness assumptions, EoS has
 014 been widely observed in deep learning, but its theoretical foundations remain in-
 015 complete. We propose a framework for analyzing EoS of non-Euclidean GD using
 016 directional smoothness (Mishkin et al., 2024), which naturally extends to non-
 017 Euclidean norms. This approach allows us to characterize EoS beyond the stan-
 018 dard Euclidean setting, encompassing methods such as ℓ_∞ -descent, Block CD,
 019 Spectral GD, and Muon without momentum. We derive the appropriate measure
 020 of the generalized sharpness under an arbitrary norm. Our generalized sharpness
 021 measure includes previously studied vanilla GD and preconditioned GD as special
 022 cases. Through analytical results and experiments on neural networks, we show
 023 that non-Euclidean GD also exhibits progressive sharpening followed by oscilla-
 024 tions around the threshold $2/\eta$. Practically, our framework provides a single,
 025 geometry-aware spectral measure that works across optimizers, bridging the gap
 026 between empirical observations and deep learning theory.

1 INTRODUCTION

029 In supervised settings, training machine learning models is posed as empirical risk minimization
 030 $\min_{\mathbf{w} \in \mathbb{R}^d} \mathcal{L}(\mathbf{w})$, where $\mathbf{w} \in \mathbb{R}^d$ are the neural network's parameters, and $\mathcal{L}(\mathbf{w})$ is the full-batch
 031 loss, which we assume is bounded below by $\mathcal{L}^* > -\infty$. In deep learning, \mathcal{L} is typically nonconvex
 032 and highly structured (Li et al., 2018; Kim et al., 2024). Nevertheless, first-order methods such as
 033 SGD and its adaptive variants (Duchi et al., 2011; Kingma & Ba, 2014) are the workhorses of practice
 034 and scale effectively to large models, despite a limited theoretical understanding of their success.

035 Full-batch gradient descent (GD) serves as the canonical proxy for analyzing gradient-based training.
 036 Classical results for L -smooth convex objectives guarantee descent for step sizes up to $2/L$. In
 037 contrast, recent empirical work reveals a characteristic two-phase behavior when deep networks
 038 are trained with GD. In the initial phase, called the progressive sharpening phase, the loss $\mathcal{L}(\mathbf{w}_t)$
 039 decreases monotonically while the sharpness $S(\mathbf{w}_t) := \lambda_{\max}(\nabla^2 \mathcal{L}(\mathbf{w}_t))$ grows. This is followed
 040 by the edge-of-stability (EoS) phase, where the loss behaves non-monotonically yet decreases over
 041 longer horizons, while the sharpness hovers near the threshold $2/\eta$ (Cohen et al., 2021).

042 The EoS phenomenon has been found to extend beyond vanilla GD. Cohen et al. (2022) showed that
 043 adaptive preconditioning methods such as Adagrad and Adam exhibit an EoS characterization that
 044 revolves around the top eigenvalue of the *preconditioned* Hessian, while Long & Bartlett (2024)
 045 showed that SAM obeys a certain EoS characterization as well. Despite these advances, the question
 046 of how EoS generalizes to other optimizers remains underexplored. In this work, we investigate
 047 how the EoS phenomenon carries over to a broad family of optimization algorithms: that of non-
 048 Euclidean gradient descent with respect to an arbitrary norm.

049 **Definition 1.1.** For a norm $\|\cdot\|$ and a step-size $\eta > 0$, the associated non-Euclidean GD method is
 050 given by the minimization of the regularized linearization around the current point \mathbf{w}_t :

$$052 \mathbf{w}_{t+1} = \operatorname{argmin}_{\mathbf{y}} \mathcal{L}(\mathbf{w}_t) + \langle \nabla \mathcal{L}(\mathbf{w}_t), \mathbf{y} - \mathbf{w}_t \rangle + \frac{1}{2\eta} \|\mathbf{y} - \mathbf{w}_t\|^2$$

$$= \mathbf{w}_t - \eta \|\nabla \mathcal{L}(\mathbf{w}_t)\|_* (\nabla \mathcal{L}(\mathbf{w}_t))_*, \quad (1)$$

where the *dual norm* $\|\nabla \mathcal{L}(\mathbf{w}_t)\|_*$ and *dual gradient* $(\nabla \mathcal{L}(\mathbf{w}_t))_*$ are defined as:

$$\|\nabla \mathcal{L}(\mathbf{w}_t)\|_* := \max_{\|\mathbf{y}\|=1} \langle \nabla \mathcal{L}(\mathbf{w}_t), \mathbf{y} \rangle, \quad (\nabla \mathcal{L}(\mathbf{w}_t))_* := \operatorname{argmax}_{\|\mathbf{y}\|=1} \langle \nabla \mathcal{L}(\mathbf{w}_t), \mathbf{y} \rangle. \quad (2)$$

We let $\mathbf{d}_t := \|\nabla \mathcal{L}(\mathbf{w}_t)\|_* (\nabla \mathcal{L}(\mathbf{w}_t))_*$ denote the update “direction” (i.e. the update without η).

This formulation reduces to vanilla GD when the norm $\|\cdot\|$ is taken to be the ℓ_2 norm. It also subsumes methods not previously studied by prior work on EoS such as ℓ_∞ -descent (for $\|\cdot\| = \ell_\infty$) and Spectral GD (for $\|\cdot\| = \|\cdot\|_{2 \rightarrow 2}$) (Carlson et al., 2015) (which underlies the popular Muon method (Jordan et al., 2024)), as well as Block CD (Nesterov, 2012) and other coordinate descent variants.

Sometimes, the dual norm is omitted from the update (1). We refer to the resulting algorithm as *normalized* non-Euclidean GD.¹

Definition 1.2. For a norm $\|\cdot\|$ (not necessarily the ℓ_2 norm) and a step-size $\eta > 0$, the associated *normalized* non-Euclidean GD method is given by

$$\mathbf{w}_{t+1} = \mathbf{w}_t - \eta (\nabla \mathcal{L}(\mathbf{w}_t))_*, \quad (3)$$

where the dual gradient $(\nabla \mathcal{L}(\mathbf{w}_t))_*$ is defined in (2).

When $\|\cdot\|$ is the ℓ_∞ norm, this formulation recovers SignGD (Bernstein et al., 2018), and when $\|\cdot\|$ is the spectral norm $\|\cdot\|_{2 \rightarrow 2}$, it recovers Muon (Jordan et al., 2024). Our main contributions are summarized as follows:

1. We identify that an intermediary quantity called directional smoothness $D^{\|\cdot\|}(\mathbf{y}, \mathbf{w})$ (Mishkin et al., 2024) can be used to study the dynamics of sharpness and the EoS. Directional smoothness is an average curvature between two consecutive iterates.
2. Through a simple identity, we show that if the loss decreases, and the gradient norm squared is approximately stable, then directional smoothness *must* increase up to $2/\eta$. Sharpness is an (approximate) upper-bound on directional smoothness, thus when directional smoothness increases up to $2/\eta$, so will sharpness. Furthermore, if the loss oscillates, then directional smoothness must also oscillate around $2/\eta$.
3. Extending directional smoothness beyond Euclidean norm, we define a generalized sharpness $S^{\|\cdot\|}$ of GD under any norm $\|\cdot\|$. In the special cases of Euclidean and preconditioned GD, this measure recovers previously established notions of sharpness.
4. Across MLPs, CNNs, and Transformers architectures, we observe that $S^{\|\cdot\|}$ hovers around the stability threshold $2/\eta$, demonstrating EoS behavior in diverse architectures.
5. To shed light on the mechanism underlying this behavior, we analyze the dynamics of non-Euclidean GD on quadratic objectives.

1.1 RELATED WORKS

The EoS phenomenon was first documented for vanilla GD with step-size η , where the sharpness (the maximum Hessian eigenvalue) was observed to hover near the stability threshold $2/\eta$ (Cohen et al., 2021). This initial work also extended empirical observations to GD with momentum and provided intuition for EoS on quadratic objectives. Building on this, Arora et al. (2022) gave a mathematical analysis of the implicit regularization that arises at EoS, showing that in non-smooth loss landscapes the updates of normalized GD follow a deterministic flow constrained to the manifold of minimal loss. A subsequent study by Song & Yun (2023) demonstrated empirically that GD trajectories align with a universal bifurcation diagram during EoS, while Damian et al. (2022) identified self-stabilization as the key mechanism: a cubic term in the Taylor expansion along the top Hessian eigenvector introduces negative feedback that drives sharpness back toward $2/\eta$ whenever it exceeds the threshold. Beyond the stability plateau, Ghosh et al. (2025) analyzed loss oscillations in deep linear networks,

¹We refer to algorithms that satisfy Def. 1.1 and 1.2 for ℓ_∞ norm as ℓ_∞ -descent and SignGD respectively.

108 demonstrating that they happen in a low-dimensional subspace whose dimension depends on the
 109 step-size η . Finally, several works connect EoS with the catapult mechanism observed in training
 110 with a large learning rate (Lewkowycz et al., 2020; Zhu et al., 2024; Kalra & Barkeshli, 2023).

111 The phenomenon has also been studied for preconditioned and adaptive methods. Cohen et al.
 112 (2022) showed that the sharpness of the preconditioned Hessian stabilizes at the same threshold for
 113 methods such as AdaGrad and RMSprop. Meanwhile, Long & Bartlett (2024) conducted a stability
 114 analysis of SAM (Foret et al., 2020) on quadratics, empirically showing that SAM operates at the edge
 115 of stability. Extensions beyond full-batch GD include Lee & Jang (2023), who analyzed the interaction
 116 between batch-gradient distributions and loss geometry to extend EoS to SGD, and Andreyev &
 117 Beneventano (2024), who proposed an alternative stochastic counterpart of EoS.

118 Despite this progress, most prior studies have focused on a narrow family of algorithms (e.g., vanilla
 119 GD, preconditioned GD, or SAM), leaving a fundamental gap in our understanding of spectral proper-
 120 ties and raising the question of whether these insights extend to substantially different optimization
 121 methods such as Muon (Jordan et al., 2024) and SignGD (Bernstein et al., 2018). In this work, we
 122 close this gap by introducing a unified framework for analyzing EoS across optimization algorithms,
 123 leveraging the recent insight that many methods can be interpreted as variants of steepest descent
 124 under an appropriate norm (Bernstein & Newhouse, 2024).

126 2 PROGRESSIVE SHARPENING AND DIRECTIONAL SMOOTHNESS

127 Classical descent guarantees for GD rely on global L -smoothness, but such bounds are often too
 128 pessimistic for neural networks (Zhang et al., 2019). Instead, we adopt a local, trajectory-aware
 129 notion of directional smoothness (Mishkin et al., 2024).

132 **Definition 2.1.** We call a function $D^{\|\cdot\|}(\mathbf{w}_t, \mathbf{w}_{t+1})$ a valid *directional smoothness* at iteration t if

$$134 \quad \mathcal{L}(\mathbf{w}_{t+1}) \leq \mathcal{L}(\mathbf{w}_t) + \langle \nabla \mathcal{L}(\mathbf{w}_t), \mathbf{w}_{t+1} - \mathbf{w}_t \rangle + \frac{D^{\|\cdot\|}(\mathbf{w}_t, \mathbf{w}_{t+1})}{2} \|\mathbf{w}_{t+1} - \mathbf{w}_t\|^2, \quad (4)$$

136 where $D^{\|\cdot\|}(\mathbf{w}_t, \mathbf{w}_{t+1})$ depends only on the behavior of the loss \mathcal{L} along the chord $[\mathbf{w}_t, \mathbf{w}_{t+1}]$.

138 Mishkin et al. (2024) provide several examples of the directional smoothness. In this work, we
 139 choose the tightest one

$$141 \quad D^{\|\cdot\|}(\mathbf{w}, \mathbf{y}) := \frac{\mathcal{L}(\mathbf{y}) - \mathcal{L}(\mathbf{w}) - \langle \nabla \mathcal{L}(\mathbf{w}), \mathbf{y} - \mathbf{w} \rangle}{\frac{1}{2} \|\mathbf{y} - \mathbf{w}\|^2}, \quad (5)$$

144 which makes (4) hold with equality. Although this quantity might not be positive (and thus falls out-
 145 side the positivity requirements of Mishkin et al. (2024)), positivity is not required in the following
 146 presentation. Substituting one step of non-Euclidean GD into (4) yields

$$147 \quad \begin{aligned} \mathcal{L}(\mathbf{w}_{t+1}) &= \mathcal{L}(\mathbf{w}_t) - \eta \langle \nabla \mathcal{L}(\mathbf{w}_t), \mathbf{d}_t \rangle + \frac{\eta^2}{2} D^{\|\cdot\|}(\mathbf{w}_t, \mathbf{w}_{t+1}) \|\mathbf{d}_t\|_*^2 \\ 148 &= \mathcal{L}(\mathbf{w}_t) - \eta \left(1 - \frac{\eta}{2} D^{\|\cdot\|}(\mathbf{w}_t, \mathbf{w}_{t+1})\right) \|\nabla \mathcal{L}(\mathbf{w}_t)\|_*^2. \end{aligned} \quad (6)$$

151 Whenever $\|\nabla \mathcal{L}(\mathbf{w}_t)\|_* > 0$, the loss decreases if *and only if*

$$153 \quad \mathcal{L}(\mathbf{w}_{t+1}) \leq \mathcal{L}(\mathbf{w}_t) \iff D^{\|\cdot\|}(\mathbf{w}_t, \mathbf{w}_{t+1}) \leq \frac{2}{\eta}. \quad (7)$$

155 The equivalence in (7) justifies the progressive sharpening of the directional smoothness. Note that
 156 in deep learning experiments where EoS is observed, the gradient norm remains non-zero (Defazio
 157 et al., 2023; Defazio, 2025), see the Gradient Norm panel in Fig. 1. Therefore, according to (7), if the
 158 loss initially decreases and then starts to oscillate, as is often observed in training, then directional
 159 smoothness must start below $2/\eta$ and then increase (sharpen) up to $2/\eta$, and then oscillate around
 160 $2/\eta$. Indeed, see the Directional Smoothness panel in Fig. 1, where we can see that the directional
 161 smoothness progressively sharpens up to $2/\eta$. Thus, by almost definition, directional smoothness
 exhibits the sharpening and EoS phase.

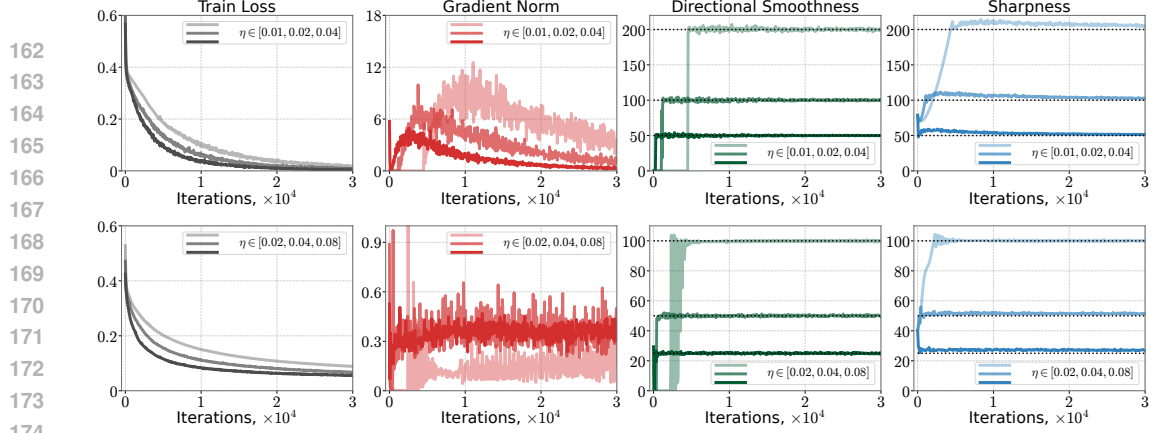


Figure 1: (Vanilla GD) Train loss, gradient norm, directional smoothness, and sharpness during training MLP (**top**) and CNN (**bottom**) models on CIFAR10-5k dataset with vanilla GD. Horizontal dashed lines correspond to the value $2/\eta$.

2.1 CONNECTION TO SHARPNESS

Next, we show how directional smoothness is closely related to a Hessian quantity that we will call the generalized sharpness. We can relate (5) to sharpness by using the 2nd-order Taylor expansion of our objective and one step of non-Euclidean GD in (1)

$$\begin{aligned} D^{\|\cdot\|}(\mathbf{w}_t, \mathbf{w}_{t+1}) &:= \frac{\mathcal{L}(\mathbf{w}_{t+1}) - \mathcal{L}(\mathbf{w}_t) - \langle \nabla \mathcal{L}(\mathbf{w}_t), \mathbf{w}_{t+1} - \mathbf{w}_t \rangle}{\frac{1}{2} \|\mathbf{w}_{t+1} - \mathbf{w}_t\|^2} \\ &= \frac{\mathbf{d}_t^\top \int_{\tau=0}^1 \nabla^2 \mathcal{L}(\mathbf{w}_t - \tau \eta \mathbf{d}_t) d\tau \mathbf{d}_t}{\|\mathbf{d}_t\|^2}. \end{aligned} \quad (8)$$

We can further upper-bound (8) by taking the maximum over all directions

$$D^{\|\cdot\|}(\mathbf{w}_t, \mathbf{w}_{t+1}) \leq \max_{\tau \in [0,1]} \frac{\mathbf{d}_t^\top \nabla^2 \mathcal{L}(\mathbf{w}_t - \tau \eta \mathbf{d}_t) \mathbf{d}_t}{\|\mathbf{d}_t\|^2} \leq \max_{\mathbf{d} \neq 0, \tau \in [0,1]} \frac{\mathbf{d}^\top \nabla^2 \mathcal{L}(\mathbf{w}_t - \tau \eta \mathbf{d}_t) \mathbf{d}}{\|\mathbf{d}\|^2}. \quad (9)$$

If we further assume that the Hessian is almost constant over the line segment $\{\mathbf{x} : \mathbf{x} = \mathbf{w}_t - \eta \tau \mathbf{d}_t, \tau \in [0, 1]\}$, we arrive at the following definition of generalized sharpness:

Definition 2.2. For any norm $\|\cdot\|$, we define the *generalized sharpness* as:

$$S^{\|\cdot\|}(\mathbf{w}) := \max_{\mathbf{d} \neq 0} \frac{\mathbf{d}^\top \nabla^2 \mathcal{L}(\mathbf{w}) \mathbf{d}}{\|\mathbf{d}\|^2} = \max_{\mathbf{d}} \mathbf{d}^\top \nabla^2 \mathcal{L}(\mathbf{w}) \mathbf{d} \quad \text{s.t. } \|\mathbf{d}\|^2 \leq 1. \quad (10)$$

The optimization problem (10) involves *maximizing* a quadratic function over a convex constraint set, and is thus challenging to solve in general. For some choices of norm $\|\cdot\|$, the problem (10) has an analytical solution (e.g., vanilla GD or Block CD). For other norms, we will heuristically approximate the solution to (10) using the Frank-Wolfe (FW) algorithm (Frank et al., 1956) run from multiple random restarts (Alg. 1). On smooth, non-convex objectives, FW is known to converge to a first-order stationary point over convex-sets with FW gap as a measure (Lacoste-Julien, 2016). Since a stationary point is not necessarily the global maximum, we repeatedly run Frank-Wolfe from multiple random restarts and then take the maximum over all trials. Empirically, we usually observe that the generalized sharpness estimated using this procedure converges to some limiting value as the number of random restarts grows. Note that in Alg. 1, we project the output of FW onto the unit norm sphere, as the final Frank-Wolfe iterate may lie in the interior of the norm ball while the true global maximizer

Algorithm 1: Frank-Wolfe to approximate (10)

Input: norm $\|\cdot\|$, $\gamma_k = \frac{2}{2+k}$, $S_0 = 0$

for *restart* $m = 1, \dots, M$ **do**

$\mathbf{u}_0 \sim \mathcal{N}(0, \mathbf{I})$, $\mathbf{u}_0 = \Pi_{\|\cdot\|=1}(\mathbf{u}_0)$

for $k = 0, 1, \dots, K-1$ **do**

$\mathbf{v}_k = \Pi_{\|\cdot\| \leq 1}(\nabla^2 \mathcal{L}(\mathbf{w}_t) \mathbf{u}_k)$

$\mathbf{u}_{k+1} = (1 - \gamma_k) \mathbf{u}_k + \gamma_k \mathbf{v}_k$

$\mathbf{u}_K = \Pi_{\|\cdot\|=1}(\mathbf{u}_K)$, $\hat{S}_m = \mathbf{u}_K^\top \nabla^2 \mathcal{L}(\mathbf{w}_t) \mathbf{u}_K$

$S_m = \max\{S_{m-1}, \hat{S}_m\}$

Output: S_M

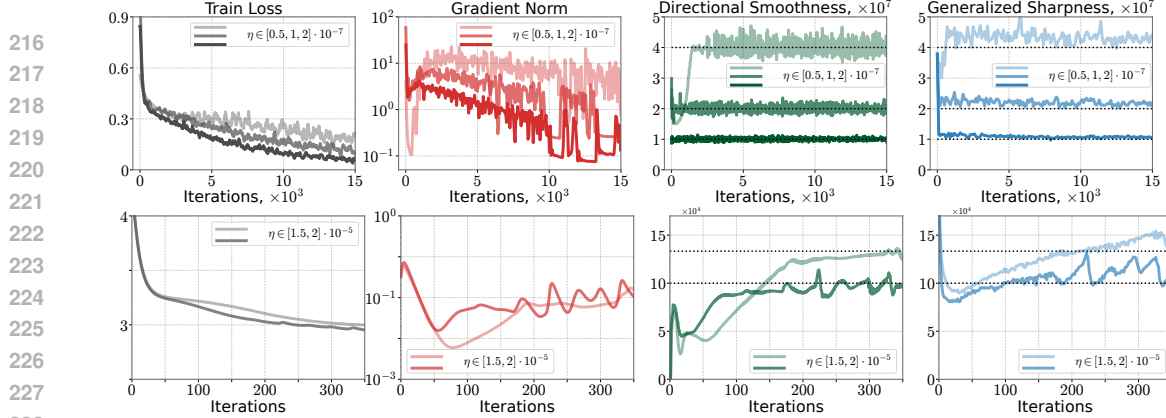


Figure 2: (ℓ_∞ -descent) Train loss, gradient norm, directional smoothness, and generalized sharpness (14) during training MLP on CIFAR10-5k (top) and Transformer on Tiny Shakespeare (bottom) with ℓ_∞ -descent. Horizontal dashed lines correspond to the value $2/\eta$.

must lie on the boundary. See App. A for a more detailed discussion of our procedure for approximating (10).

3 EXAMPLES OF NON-EUCLIDEAN GRADIENT DESCENT

We begin by showing that the generalized sharpness (10) recovers previously derived notions of sharpness, establishing the tightness of our approach. We then examine generalized sharpness under several non-Euclidean norms.

Euclidean ℓ_2 Norm. We consider a standard Euclidean ℓ_2 norm. In this case, the sharpness measure (10) can be computed explicitly. Indeed, the maximum in (10) equals the largest eigenvalue of the Hessian $\lambda_{\max}(\nabla^2 \mathcal{L}(\mathbf{w}_t))$. This result coincides with the sharpness measure introduced in Cohen et al. (2021). In Fig. 1, we report the training dynamics of vanilla GD, flattening all parameters of the networks. We observe that the directional smoothness and sharpness hover at $2/\eta$ when the algorithm enters EoS stage, supporting our claims in (7).

Preconditioned ℓ_2 Norm. Let $\mathbf{P}_t \in \mathbb{R}^{d \times d}$ be a symmetric positive definite matrix, which we will use as a preconditioner. That is, we define the preconditioned ℓ_2 norm (also referred to as the Mahalanobis distance) by $\|\mathbf{w}\|_{\mathbf{P}_t}^2 := \langle \mathbf{P}_t \mathbf{w}, \mathbf{w} \rangle = \|\mathbf{P}_t^{1/2} \mathbf{w}\|_2^2$. Under this norm, preconditioned GD (1) is given by

$$\mathbf{w}_{t+1} = \mathbf{w}_t - \eta \mathbf{P}_t^{-1} \nabla \mathcal{L}(\mathbf{w}_t). \quad (11)$$

This case includes Adagrad (Duchi et al., 2011), RMSProp (Tieleman & Hinton, 2012) and Newton’s method as special cases. According to (10), the correct notion of sharpness for this norm is given by

$$S^{\|\cdot\|_{\mathbf{P}_t}}(\mathbf{w}) := \max_{\mathbf{d} \neq 0} \frac{\mathbf{d}^\top \nabla^2 \mathcal{L}(\mathbf{w}) \mathbf{d}}{\|\mathbf{d}\|_{\mathbf{P}_t}^2} = \max_{\mathbf{v} \neq 0} \frac{\mathbf{v}^\top \mathbf{P}_t^{-1/2} \nabla^2 \mathcal{L}(\mathbf{w}) \mathbf{P}_t^{-1/2} \mathbf{v}}{\|\mathbf{v}\|_2^2}, \quad (12)$$

where we arrived at last equality by using the change of variables $\mathbf{v} = \mathbf{P}_t^{1/2} \mathbf{d}$. This definition matches the sharpness definition for preconditioned GD given in (Cohen et al., 2025).

Infinity ℓ_∞ Norm. In this case, we consider the infinity norm over the parameters of the neural network, that is $\|\mathbf{w}\|_\infty := \max_{j \in [d]} |\mathbf{w}_j|$. The resulting method (1) is the following variant of ℓ_∞ -descent given by

$$\mathbf{w}_{t+1} = \mathbf{w}_t - \eta \|\nabla \mathcal{L}(\mathbf{w}_t)\|_1 \text{sign}(\nabla \mathcal{L}(\mathbf{w}_t)), \quad (13)$$

The corresponding definition of sharpness (10) under this norm is given by

$$S^{\|\cdot\|_\infty}(\mathbf{w}) = \max_{\mathbf{d} \neq 0} \frac{\mathbf{d}^\top \nabla^2 \mathcal{L}(\mathbf{w}) \mathbf{d}}{\|\mathbf{d}\|_\infty^2} = \max_{\mathbf{d}} \mathbf{d}^\top \nabla^2 \mathcal{L}(\mathbf{w}) \mathbf{d} \quad \text{s.t. } \|\mathbf{d}\|_\infty \leq 1. \quad (14)$$

The optimization problem (14) has also appeared in statistical physics, where it is equivalent to finding the maximum energy—or, correspondingly, the *ground state* in a *flipped sign* formulation—of

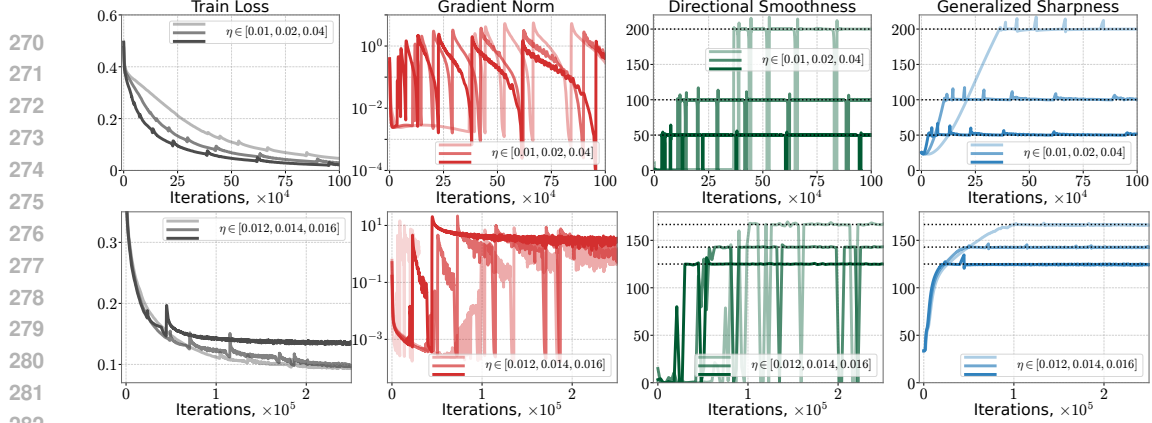


Figure 3: (Block CD) Train loss, gradient norm, directional smoothness, and generalized sharpness (16) during training MLP (top) and CNN (bottom) models on CIFAR10-5k dataset with Block CD. Horizontal dashed lines correspond to the value $2/\eta$.

an Ising spin glass on the hypercube. This corresponds to maximizing the Hamiltonian over binary spin assignments $d_i = \pm 1$. The problem is known to be NP-hard in general (Zhang & Kamenev, 2025; Kochenberger et al., 2014). Therefore, we use Alg. 1 to approximate (14), with the projection operator being $\Pi_{\|\cdot\|_\infty=1}(\cdot) \equiv \text{sign}(\cdot)$.

Fig. 2 presents the convergence results of ℓ_∞ -descent, applied to the flattened networks' parameters. In this case, directional smoothness plateaus at $2/\eta$. A similar behavior appears for generalized sharpness. We observe several interesting phenomena. First, in some cases, the generalized sharpness hovers *slightly above* the stability threshold $2/\eta$. As we review in App. C, a similar effect has been observed for Euclidean GD when there are multiple Hessian eigenvalues at the edge of stability, and we hypothesize this behavior could have a similar origin. Second, FW requires a sufficient number of restarts to obtain a good approximation of the generalized sharpness in (14): see Fig. F.2.

Block $\ell_{1,2}$ Norm. In this case, we take into account the block-wise structure of neural networks. Let the parameters \mathbf{w} be split into L blocks, i.e., $\mathbf{w} = (\mathbf{w}^1, \dots, \mathbf{w}^L) \in \mathbb{R}^{d_1} \oplus \mathbb{R}^{d_2} \dots \oplus \mathbb{R}^{d_L}$ where $\sum_{\ell=1}^L d_\ell = d$. We consider GD in $\|\cdot\|_{1,2}$ norm² defined as $\|\mathbf{w}\|_{1,2} := \sum_{\ell=1}^L \|\mathbf{w}^\ell\|_2$. Let $\ell_{\max} := \text{argmax}_{\ell \in [L]} \|\nabla_{\mathbf{w}^\ell} \mathcal{L}(\mathbf{w}_t)\|$. Then GD in this norm reduces to Block CD

$$\mathbf{w}_{t+1}^{\ell_{\max}} = \mathbf{w}_t^{\ell_{\max}} - \eta \nabla_{\mathbf{w}^{\ell_{\max}}} \mathcal{L}(\mathbf{w}_t), \quad \mathbf{w}_{t+1}^\ell = \mathbf{w}_t^\ell \quad \text{for } \ell \neq \ell_{\max}. \quad (15)$$

The derivations of GD in this norm are given in Lemma D.5. The corresponding definition of sharpness (10) under this norm is given by

$$S^{\|\cdot\|_{1,2}}(\mathbf{w}_t) = \max_{\mathbf{d} \neq 0} \frac{\langle \mathbf{d}, \nabla^2 \mathcal{L}(\mathbf{w}_t) \mathbf{d} \rangle}{\|\mathbf{d}\|_{1,2}^2} = \max_{\mathbf{d}} \langle \mathbf{d}, \nabla^2 \mathcal{L}(\mathbf{w}_t) \mathbf{d} \rangle \quad \text{s.t. } \|\mathbf{d}\|_{1,2} \leq 1. \quad (16)$$

The solution to (16) can be given explicitly if the Hessian $\nabla^2 \mathcal{L}(\mathbf{w}_t)$ is PSD (see Lemma D.8)

$$S^{\|\cdot\|_{1,2}}(\mathbf{w}) = \max_{\ell \in [L]} \lambda_{\max}(\nabla_{\mathbf{w}^\ell}^2 \mathcal{L}(\mathbf{w})). \quad (17)$$

However, for the general $\nabla^2 \mathcal{L}(\mathbf{w}_t)$, solving (16) is NP-hard (Bhattiprolu et al., 2021), but still can be approximated by the FW algorithm. The exact steps of FW in this case are derived in Lemma D.9.

Figure 3 shows the convergence of Block CD, where we adopt the natural block-wise structure of the network – each block corresponding to a weight matrix or bias vector of a layer. The generalized sharpness, which is approximated by the maximum eigenvalue of each block of the Hessian, approaches the threshold $2/\eta$, supporting our theoretical observations. In contrast, the directional smoothness curves display sharper dynamics: while they also reach $2/\eta$, they exhibit sudden drops whenever training shifts from a layer already at the EoS regime to one that has not yet reached it. These drops are also mirrored in the gradient norm dynamics. Similar to ℓ_∞ , FW algorithm is sensitive to the number of restarts M . Fig. G.1 reports that FW with $M = 10$ provides a stable estimation of the generalized sharpness, while FW with $M = 1$ does not.

²In this case, each block \mathbf{w}^ℓ is treated as a vector.

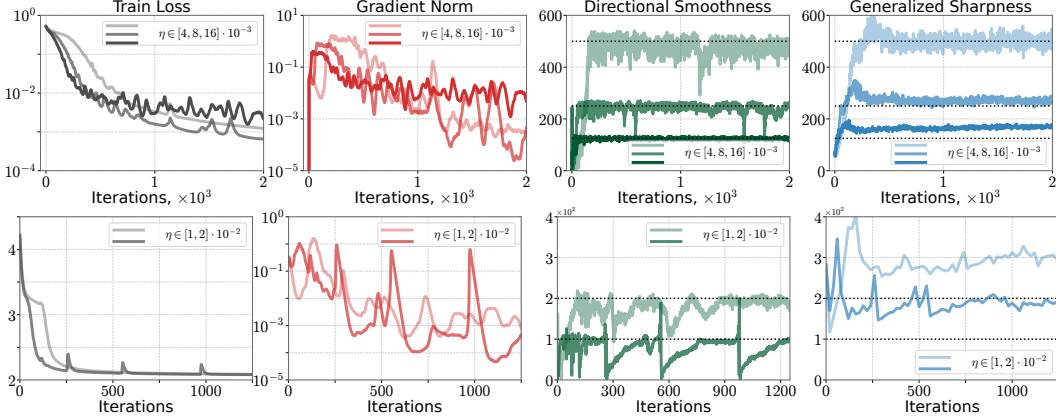


Figure 4: (Spectral GD) Train loss, gradient norm, directional smoothness, and generalized sharpness (19) during training MLP (top, CIFAR10) and Transformer (bottom, Tiny Shakespeare) models with the Spectral GD. Horizontal dashed lines correspond to the value $2/\eta$.

Spectral $\|\cdot\|_{2 \rightarrow 2}$ Norm. To handle matrix norms, we shift perspective and treat the layers of the network as blocks of matrices³ $\mathbf{W} := (\mathbf{W}^1, \dots, \mathbf{W}^L)$. In this setting, the natural inner product is the matrix trace $\langle \mathbf{W}, \mathbf{G} \rangle := \text{tr}(\mathbf{W}^\top \mathbf{G})$. In this framework, one may endow each block \mathbf{W}^ℓ with a matrix norm, and then define a global norm on \mathbf{W} by specifying an aggregation rule across layers. One particularly neat choice Bernstein & Newhouse (2024) is max over the spectral norms $\|\mathbf{W}\|_{\infty,2} := \max_{\ell \in [L]} \|\mathbf{W}^\ell\|_2$, where $\|\mathbf{W}^\ell\|_2 := \max_{\|\mathbf{d}\|_2=1} \|\mathbf{W}^\ell \mathbf{d}\|_2$. Under this geometry, GD aligns with the top singular directions of each layer. Concretely, the update is

$$\mathbf{W}_{t+1}^\ell = \mathbf{W}_t^\ell - \eta \gamma \mathbf{U}_t^\ell \mathbf{V}_t^\ell, \quad \gamma = \sum_{\ell=1}^L \text{tr}(\Sigma_t^\ell), \quad (18)$$

where $\mathbf{U}_t^\ell \Sigma_t^\ell \mathbf{V}_t^\ell = \nabla_{\mathbf{W}^\ell} \mathcal{L}(\mathbf{W}_t)$ is the reduced SVD of the gradient of the ℓ -th layer. The product $\mathbf{U}_t^\ell \mathbf{V}_t^\ell$ is also known as the polar factor of the matrix $\nabla_{\mathbf{W}^\ell} \mathcal{L}(\mathbf{W}_t)$, which can be computed efficiently on GPU using variants of the Newton-Schulz method (Jordan et al., 2024; Higham, 1986) or the PolarExpress (Amsel et al., 2025). The corresponding definition of sharpness (10) under this norm is given by

$$S^{\|\cdot\|_{2 \rightarrow 2}}(\mathbf{W}) = \max_{\mathbf{D} \neq 0} \frac{\langle \mathbf{D}, \nabla^2 \mathcal{L}(\mathbf{W}_t)[\mathbf{D}] \rangle}{\|\mathbf{D}\|_{\infty,2}^2} = \max_{\mathbf{D}} \langle \mathbf{D}, \nabla^2 \mathcal{L}(\mathbf{W})[\mathbf{D}] \rangle \quad (19)$$

s.t. $\|\mathbf{D}^\ell\|_2 \leq 1 \forall \ell \in [L]$,

where the operator $\nabla^2 \mathcal{L}(\mathbf{W})[\mathbf{D}]$ is the directional derivative of the gradient $\nabla^2 \mathcal{L}(\mathbf{W}_t)[\mathbf{D}] := \frac{d}{d\epsilon} \nabla \mathcal{L}(\mathbf{W}_t + \epsilon \mathbf{D})|_{\epsilon=0}$. This is exactly the operation computed by Hessian-vector-product in PyTorch (Paszke et al., 2019). The solution to (19) cannot be computed explicitly. Therefore, we rely on the FW algorithm to approximate it. The exact steps of FW are derived in Lemma D.4.

Fig. 4 presents the convergence dynamics of Spectral GD. As in previous cases, both directional smoothness and generalized sharpness approach the stability threshold $2/\eta$. Notably, as with the ℓ_∞ norm, the generalized sharpness gradually reaches this threshold but remains slightly above it. However, in contrast to ℓ_∞ and $\ell_{1,2}$ norms, FW is not sensitive to the number of restarts M (Fig. H.2).

4 NORMALIZED NON-EUCLIDEAN GRADIENT DESCENT

In this section, we demonstrate that our theoretical observations extend to normalized non-Euclidean GD. In more detail, the normalized update rule (3) with step-size η can be rewritten as the unnormalized update rule (1) with effective step-size $\tilde{\eta} = \frac{\eta}{\|\nabla \mathcal{L}(\mathbf{w}_t)\|_*}$. Therefore, the corresponding directional smoothness $D^{\|\cdot\|}(\mathbf{w}_t, \mathbf{w}_{t+1})$ and generalized sharpness of normalized non-Euclidean GD hovers at the threshold $\frac{2}{\tilde{\eta}} = \frac{2\|\nabla \mathcal{L}(\mathbf{w}_t)\|_*}{\eta}$. This can also be derived by substituting one step of normalized non-Euclidean GD into (5), giving

$$\mathcal{L}(\mathbf{w}_{t+1}) = \mathcal{L}(\mathbf{w}_t) - \eta \left(\|\nabla \mathcal{L}(\mathbf{w}_t)\|_* - \frac{\eta}{2} D^{\|\cdot\|}(\mathbf{w}_t, \mathbf{w}_{t+1}) \right). \quad (20)$$

³We use upper case notation to highlight the matrix structure.

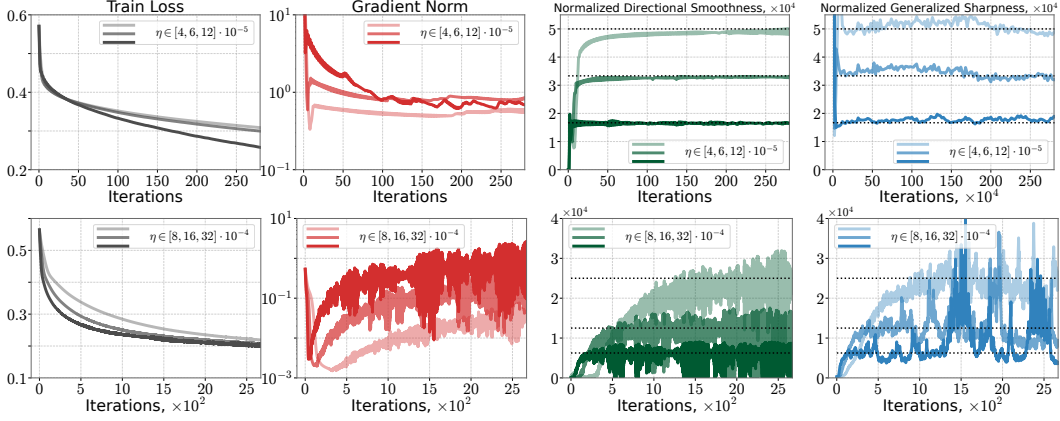


Figure 5: (Normalized non-Euclidean GD) Gradient norm, train loss, directional smoothness (normalized by the dual gradient norm), and generalized sharpness (normalized by the dual gradient norm) during training a CNN model with SignGD (CIFAR10-5k dataset, top line) and Muon without momentum (CIFAR10 dataset, bottom line). Horizontal dashed lines correspond to the value $2/\eta$.

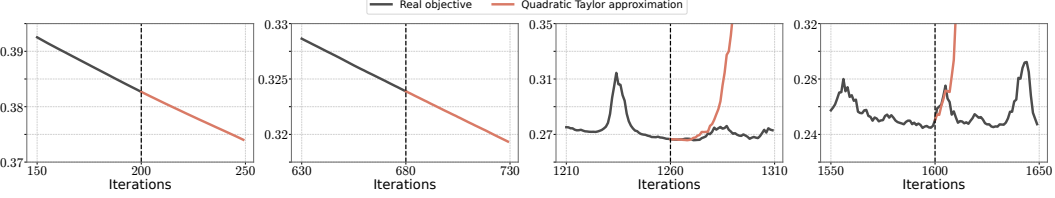


Figure 6: MSE loss ($\eta = 0.002$). At four marked iterations, we switch Spectral GD when training CNN on CIFAR10 from the true objective to its quadratic Taylor approximation at the current iterate (orange). (Two left, before EoS), the quadratic closely tracks the true loss; (two right, during EoS, it quickly diverges.

Therefore, the loss decreases if *and only if*

$$\mathcal{L}(\mathbf{w}_{t+1}) \leq \mathcal{L}(\mathbf{w}_t) \iff D^{\|\cdot\|}(\mathbf{w}_t, \mathbf{w}_{t+1}) \leq 2\|\nabla \mathcal{L}(\mathbf{w}_t)\|_*/\eta. \quad (21)$$

The derivations in Sec. 2.1 applies to normalized non-Euclidean GD. Fig. 5 empirically confirms the claims for SignGD and Muon, extending our EoS observations to practical algorithms. We demonstrate that the directional smoothness and generalized sharpness normalized by the dual gradient norm, i.e., $\frac{D^{\|\cdot\|}(\mathbf{w}_t, \mathbf{w}_{t+1})}{\|\nabla \mathcal{L}(\mathbf{w}_t)\|_*}$ and $\frac{S^{\|\cdot\|}(\mathbf{w}_t)}{\|\nabla \mathcal{L}(\mathbf{w}_t)\|_*}$ respectively, hover at the stability threshold $2/\eta$.

5 TOWARDS UNDERSTANDING THE UNDERLYING MECHANISM

For Euclidean GD, the EoS dynamics are partly understood. The significance of the sharpness $\lambda_{\max}(\nabla^2 \mathcal{L}(\mathbf{w}_t))$ is that it determines whether or not GD is divergent on the local quadratic Taylor approximation. Indeed, if GD with step size η is run on any quadratic objective function where the Hessian matrix has any eigenvalue(s) greater than $2/\eta$, then GD will oscillate with exponentially growing magnitude along the corresponding eigenvector(s). This will occur starting from almost any initialization (the one exception being if the iterate is initialized to be *exactly* orthogonal to the top eigenvector(s), an event which occurs with probability zero under any typical random initialization). Accordingly, on neural network objectives, once progressive sharpening drives the sharpness above $2/\eta$, the iterate starts to oscillate with growing magnitude along any unstable eigenvectors, just as one would expect based on the local quadratic Taylor approximation. These oscillations cause the loss to (temporarily) increase, and the directional smoothness to exceed $2/\eta$. The oscillations also crucially induce reduction of sharpness, as is revealed by considering a local cubic Taylor expansion (Damian et al., 2022), an effect which prevents the sharpness from rising further and thereby stabilizes training.

For non-Euclidean GD, since we observe that the generalized sharpness (10) (or at least, our estimate of it) hovers near $2/\eta$, it is natural to ask if an analogous explanation holds. Standard arguments from convex optimization give the following result.

432
433
434
435

Theorem 5.1. Let $\mathcal{L}(\mathbf{w}) := \frac{1}{2}\mathbf{w}^\top \mathbf{H}\mathbf{w}$ for some $\mathbf{H} \succ 0$. For some norm $\|\cdot\|$, define the generalized sharpness $S = S^{\|\cdot\|} := \max_{\|\mathbf{d}\| \leq 1} \mathbf{d}^\top \mathbf{H}\mathbf{d}$. If we run non-Euclidean GD (Def. 1.1) on \mathcal{L} with any step-size $\eta < 2/S$, it will converge at a linear rate starting from any initial point \mathbf{w}_0 .

436
437
438
439
440
441

See App. E for the proof. This theorem generalizes, to non-Euclidean norms, the fact that GD is convergent on quadratic functions so long as the sharpness is less than $2/\eta$. However, for the Euclidean norm, the key point is that the converse is also true: gradient descent *diverges* on quadratics if the sharpness is *greater* than $2/\eta$. We now show that this property also carries over, to an extent, to the non-Euclidean setting.

442
443
444
445

Theorem 5.2. Let $\mathcal{L}(\mathbf{w}) := \frac{1}{2}\mathbf{w}^\top \mathbf{H}\mathbf{w}$ for some $\mathbf{H} \succ 0$. For some norm $\|\cdot\|$, define the generalized sharpness $S := \max_{\|\mathbf{d}\| \leq 1} \mathbf{d}^\top \mathbf{H}\mathbf{d}$. If we run non-Euclidean GD (Def. 1.1) on \mathcal{L} , there exists an initialization \mathbf{w}_0 from which GD will diverge for any step-size $\eta > 2/S$.

446
447
448
449

The full proof is in App. E, and the crux is the following lemma, which implies that the direction $\hat{\mathbf{d}}$ which attains the argmax in the generalized sharpness optimization problem is an invariant direction under the non-Euclidean GD update:

450
451

Lemma 5.3. If $\hat{\mathbf{d}} \in \arg \max_{\|\mathbf{d}\|=1} \mathbf{d}^\top \mathbf{H}\mathbf{d}$, then $(\mathbf{H}\hat{\mathbf{d}})_* = \hat{\mathbf{d}}$.

452

As a result, if the iterate is initialized in $\mathbf{w}_0 \in \text{span}(\hat{\mathbf{d}})$, then the evolution of \mathbf{w}_t is given by:

453

$$\mathbf{w}_t = (1 - \eta S)^t \mathbf{w}_0. \quad (22)$$

454
455
456
457
458

When $\eta > 2/S \iff S > 2/\eta$, these dynamics oscillate with growing magnitude and diverge. However, we note that Th. 5.2 is less strong than what is true for Euclidean GD, as Euclidean GD diverges from all but a zero-measure set of initializations, whereas Th. 5.2 only establishes divergence when the initialization is on a particular line.

459
460
461
462
463
464
465

Empirically, we can assess whether non-Euclidean GD is indeed divergent on the quadratic Taylor approximation when operating on the edge of stability. In Fig. 6, for points during training both before and after entering EoS, we switch from running non-Euclidean GD on the real objective to running non-Euclidean GD on the quadratic Taylor approximation (similar to App. E from Cohen et al. (2021)). We observe that GD is stable before reaching EoS, but divergent afterwards. This supports the idea that the significance of the generalized sharpness hovering around $2/\eta$ is related to the dynamics becoming divergent on the local quadratic Taylor approximation.

466
467
468
469

Nevertheless, we note that our explanation of this behavior is not fully satisfying, as our theory only proves that non-Euclidean EoS is divergent under a specific initialization, whereas in practice we observe that this divergence seems to occur quite generically. Bridging this gap would be an interesting question for future work.

470
471
472
473
474
475
476
477
478

It is worth highlighting an additional point of difference between the Euclidean and non-Euclidean cases. For Euclidean GD, the directional smoothness only starts to grow from ≈ 0 to $2/\eta$ *after* the sharpness crosses $2/\eta$. By contrast, for non-Euclidean GD under some norms (in particular, ℓ_∞ and $\|\cdot\|_{2 \rightarrow 2}$), we observe that the directional smoothness starts to climb towards $2/\eta$ *before* the generalized sharpness has reached $2/\eta$ (Appendix B). During this period, we find that the iterates oscillate in weight space, but the dynamics are not yet divergent on the quadratic Taylor approximation. This suggests an intermediate regime between stability and EoS regimes, which does not occur for Euclidean GD. Understanding this behavior would be an interesting question for future work.

479
480

6 CONCLUSION AND FUTURE WORK

481
482
483
484
485

We extend EoS to previously unstudied methods such as Spectral GD, ℓ_∞ -descent, and Muon, but several questions remain: (i) the mechanism underlying stability at the $2/\eta$ threshold for general non-Euclidean GD; (ii) the differing dynamics of directional smoothness in Euclidean vs. non-Euclidean GD, including a possible intermediate regime between stability and EoS; and (iii) stronger convergence theory for non-Euclidean GD on quadratics, especially when $\eta > 2/S$ for arbitrary initialization.

486 REPRODUCIBILITY STATEMENT
487488 Our code base is built upon a publicly available repository (Cohen et al., 2021), incorporating nec-
489 essary algorithms in the code base. All experiments utilize publicly available datasets, cited accord-
490 ingly. Further details are reported in the Appendix.
491492 ETHICS STATEMENT
493494 This paper presents work whose goal is to advance the field of Machine Learning. There are many
495 potential societal consequences of our work, none of which we feel must be specifically highlighted
496 here.
497498 REFERENCES
499500 Noah Amsel, David Persson, Christopher Musco, and Robert M Gower. The polar express:
501 Optimal matrix sign methods and their application to the muon algorithm. *arXiv preprint*
502 *arXiv:2505.16932*, 2025. (Cited on page 7)503 Arseniy Andreyev and Pierfrancesco Beneventano. Edge of stochastic stability: Revisiting the edge
504 of stability for sgd. *arXiv preprint arXiv:2412.20553*, 2024. (Cited on page 3)506 Sanjeev Arora, Zhiyuan Li, and Abhishek Panigrahi. Understanding gradient descent on the edge
507 of stability in deep learning. In *International Conference on Machine Learning*, 2022. (Cited on
508 page 2)509 Jeremy Bernstein and Laker Newhouse. Old optimizer, new norm: An anthology. *arXiv preprint*
510 *arXiv:2409.20325*, 2024. (Cited on pages 3, 7, 17, and 18)512 Jeremy Bernstein, Yu-Xiang Wang, Kamyar Azizzadenesheli, and Animashree Anandkumar.
513 signsgd: Compressed optimisation for non-convex problems. In *International conference on*
514 *machine learning*, pp. 560–569. PMLR, 2018. (Cited on pages 2 and 3)515 Vijay Bhattiprolu, Euiwoong Lee, and Assaf Naor. A framework for quadratic form maximization
516 over convex sets through nonconvex relaxations. In *Proceedings of the 53rd Annual ACM SIGACT*
517 *Symposium on Theory of Computing*, 2021. (Cited on page 6)518 Samuel Burer and Adam N Letchford. On nonconvex quadratic programming with box constraints.
519 *SIAM Journal on Optimization*, 2009. (Cited on pages 13 and 14)521 David Carlson, Volkan Cevher, and Lawrence Carin. Stochastic Spectral Descent for Restricted
522 Boltzmann Machines. In *Proceedings of the Eighteenth International Conference on Artificial*
523 *Intelligence and Statistics*, 2015. (Cited on page 2)524 Jeremy M. Cohen, Simran Kaur, Yuanzhi Li, J. Zico Kolter, and Ameet Talwalkar. Gradient de-
525 scent on neural networks typically occurs at the edge of stability. In *International Conference on*
526 *Learning Representations (ICLR)*, 2021. (Cited on pages 1, 2, 5, 9, 10, 15, and 25)528 Jeremy M. Cohen, Behrooz Ghorbani, Shankar Krishnan, Naman Agarwal, Sourabh Medapati,
529 Michal Badura, Daniel Suo, David Cardoze, Zachary Nado, George E Dahl, et al. Adaptive gra-
530 dient methods at the edge of stability. *arXiv preprint arXiv:2207.14484*, 2022. (Cited on pages 1,
531 3, and 28)532 Jeremy M. Cohen, Alex Damian, Ameet Talwalkar, Zico Kolter, and Jason D. Lee. Understanding
533 optimization in deep learning with central flows. *arXiv preprint arXiv:2410.24206*, 2024. (Cited
534 on page 14)535 Jeremy M. Cohen, Alex Damian, Ameet Talwalkar, Zico Kolter, and Jason D. Lee. Understand-
536 ing optimization in deep learning with central flows. In *International Conference on Learning*
537 *Representations (ICLR)*, 2025. (Cited on pages 5 and 15)539 Alex Damian, Eshaan Nichani, and Jason D. Lee. Self-stabilization: The implicit bias of gradient
540 descent at the edge of stability. *arXiv preprint arXiv:2209.15594*, 2022. (Cited on pages 2 and 8)

540 Aaron Defazio. Why gradients rapidly increase near the end of training. *arXiv preprint*
 541 *arXiv:2506.02285*, 2025. (Cited on page 3)

542

543 Aaron Defazio, Ashok Cutkosky, Harsh Mehta, and Konstantin Mishchenko. Optimal linear decay
 544 learning rate schedules and further refinements. *arXiv preprint arXiv:2310.07831*, 2023. (Cited
 545 on page 3)

546 John Duchi, Elad Hazan, and Yoram Singer. Adaptive subgradient methods for online learning
 547 and stochastic optimization. In *Proceedings of the 24th Annual Conference on Learning Theory*
 548 (*COLT*), 2011. (Cited on pages 1 and 5)

549

550 Pierre Foret, Ariel Kleiner, Hossein Mobahi, and Behnam Neyshabur. Sharpness-aware minimiza-
 551 tion for efficiently improving generalization. *arXiv preprint arXiv:2010.01412*, 2020. (Cited on
 552 page 3)

553 Marguerite Frank, Philip Wolfe, et al. An algorithm for quadratic programming. *Naval research*
 554 *logistics quarterly*, 1956. (Cited on page 4)

555 Avrajit Ghosh, Soo Min Kwon, Rongrong Wang, Saiprasad Ravishankar, and Qing Qu. Learning
 556 dynamics of deep matrix factorization beyond the edge of stability. In *The Second Conference on*
 557 *Parsimony and Learning (Recent Spotlight Track)*, 2025. (Cited on page 2)

558

559 Gene H. Golub and Charles F. Van Loan. *Matrix Computations*. Johns Hopkins University Press,
 560 4th edition, 2013. (Cited on page 14)

561 Kaiming He, Xiangyu Zhang, Shaoqing Ren, and Jian Sun. Deep residual learning for image recog-
 562 nition. In *Proceedings of the IEEE conference on computer vision and pattern recognition*, 2016.
 563 (Cited on pages 25 and 27)

564 Nicholas J Higham. Computing the polar decomposition—with applications. *SIAM Journal on*
 565 *Scientific and Statistical Computing*, 1986. (Cited on page 7)

566

567 Reiner Horst, Panos M Pardalos, and Nguyen Van Thoai. *Introduction to global optimization*.
 568 Springer Science & Business Media, 2000. (Cited on page 13)

569

570 Like Hui and Mikhail Belkin. Evaluation of neural architectures trained with square loss vs cross-
 571 entropy in classification tasks. *arXiv preprint arXiv:2006.07322*, 2020. (Cited on page 26)

571

572 Keller Jordan, Yuchen Jin, Vlado Boza, Jiacheng You, Franz Cesista, Laker Newhouse, and Jeremy
 573 Bernstein. Muon: An optimizer for hidden layers in neural networks, 2024. URL <https://kellerjordan.github.io/posts/muon/>. (Cited on pages 2, 3, and 7)

574

575 Dayal Singh Kalra and Maissam Barkeshli. Phase diagram of early training dynamics in deep
 576 neural networks: effect of the learning rate, depth, and width. *Advances in Neural Information*
 577 *Processing Systems*, 2023. (Cited on page 3)

578

579 Sungyoon Kim, Aaron Mishkin, and Mert Pilanci. Exploring the loss landscape of regularized neural
 580 networks via convex duality. *arXiv preprint arXiv:2411.07729*, 2024. (Cited on page 1)

581

582 Diederik P Kingma and Jimmy Ba. Adam: A method for stochastic optimization. *arXiv preprint*
 583 *arXiv:1412.6980*, 2014. (Cited on page 1)

584

585 Gary Kochenberger, Jin-Kao Hao, Fred Glover, Mark Lewis, and Zhipeng Lu. The unconstrained
 586 binary quadratic programming problem: a survey. *Journal of Combinatorial Optimization*, 2014.
 587 (Cited on page 6)

588

589 Alex Krizhevsky and Geoffrey Hinton. Learning multiple layers of features from tiny images. Tech-
 590 nical report, Technical Report, University of Toronto, 2009. (Cited on pages 24 and 26)

591

592 Simon Lacoste-Julien. Convergence rate of frank-wolfe for non-convex objectives. *arXiv preprint*
 593 *arXiv:1607.00345*, 2016. (Cited on pages 4 and 14)

594

595 Sungyoon Lee and Cheongjae Jang. A new characterization of the edge of stability based on a
 596 sharpness measure aware of batch gradient distribution. In *The Eleventh International Conference*
 597 *on Learning Representations*, 2023. (Cited on page 3)

594 Aitor Lewkowycz, Yasaman Bahri, Ethan Dyer, Jascha Sohl-Dickstein, and Guy Gur-Ari. The large
 595 learning rate phase of deep learning: the catapult mechanism. *arXiv preprint arXiv:2003.02218*,
 596 2020. (Cited on page 3)

597

598 Hao Li, Zheng Xu, Gavin Taylor, Christoph Studer, and Tom Goldstein. Visualizing the loss land-
 599 scape of neural nets. *Advances in neural information processing systems*, 2018. (Cited on page 1)

600 Philip M Long and Peter L Bartlett. Sharpness-aware minimization and the edge of stability. *Journal*
 601 *of Machine Learning Research*, 2024. (Cited on pages 1 and 3)

602

603 Aaron Mishkin, Ahmed Khaled, Yuanhao Wang, Aaron Defazio, and Robert M. Gower. Directional
 604 smoothness and gradient methods: Convergence and adaptivity. In *The Thirty-eighth Annual*
 605 *Conference on Neural Information Processing Systems*, 2024. (Cited on pages 2 and 3)

606 Yu. Nesterov. Efficiency of coordinate descent methods on huge-scale optimization problems. *SIAM*
 607 *Journal on Optimization*, 2012. (Cited on page 2)

608

609 Adam Paszke, Sam Gross, Francisco Massa, Adam Lerer, James Bradbury, Gregory Chanan, Trevor
 610 Killeen, Zeming Lin, Natalia Gimelshein, Luca Antiga, et al. Pytorch: An imperative style, high-
 611 performance deep learning library. *Advances in neural information processing systems*, 2019.
 612 (Cited on page 7)

613 Karen Simonyan and Andrew Zisserman. Very deep convolutional networks for large-scale image
 614 recognition. *arXiv preprint arXiv:1409.1556*, 2014. (Cited on pages 25 and 27)

615

616 Minhak Song and Chulhee Yun. Trajectory alignment: understanding the edge of stability phe-
 617 nomenon via bifurcation theory. *arXiv preprint arXiv:2307.04204*, 2023. (Cited on page 2)

618 Tijmen Tieleman and Geoffrey Hinton. Lecture 6.5—rmsprop: Divide the gradient by a running
 619 average of its recent magnitude. [http://www.cs.toronto.edu/~tijmen/csc321/](http://www.cs.toronto.edu/~tijmen/csc321/slides/lecture_slides_lec6.pdf)
 620 *slides/lecture_slides_lec6.pdf*, 2012. Coursera Lecture: Neural Networks for Ma-
 621 chine Learning. (Cited on page 5)

622

623 Hao Zhang and Alex Kamenev. On computational complexity of 3d ising spin glass: Lessons from
 624 d-wave annealer. *arXiv preprint arXiv:2501.01107*, 2025. (Cited on page 6)

625

626 Jingzhao Zhang, Tianxing He, Suvrit Sra, and Ali Jadbabaie. Why gradient clipping accelerates
 627 training: A theoretical justification for adaptivity. *arXiv preprint arXiv:1905.11881*, 2019. (Cited
 628 on page 3)

629

630 Libin Zhu, Chaoyue Liu, Adityanarayanan Radhakrishnan, and Mikhail Belkin. Catapults in sgd:
 631 spikes in the training loss and their impact on generalization through feature learning. In *Pro-
 632 ceedings of the 41st International Conference on Machine Learning*, 2024. (Cited on page 3)

633

634

635

636

637

638

639

640

641

642

643

644

645

646

647

648 649 650 651 652 653 654 655 656 657 658 659 660 661 662 663 664 665 666 667 668 669 670 671 672 673 674 675 676 677 678 679 680 681 682 683 684 685 686 687 688 689 690 691 692 693 694 695 696 697 698 699 700 701 Appendix

648	CONTENTS	
649		
650		
651		
652		
653	A Discussion on Frank-Wolfe Algorithm	13
654		
655	B An oscillatory regime before EOS	14
656		
657		
658	C The gap between the generalized sharpness and $2/\eta$	15
659		
660	D Useful Lemmas	15
661		
662	D.1 Missing Proofs for the Spectral Block Norm $\ell_{\infty,2}$	15
663	D.2 Missing Proofs for the Block $\ell_{1,2}$ Norm	18
664		
665	E Non-Euclidean Gradient Descent on Quadratics	20
666		
667	F Additional Experimental Results with ℓ_{∞} Descent	24
668		
669	F.1 Convergence When Training CNN Model	24
670	F.2 Sensitivity of Frank-Wolfe Algorithm in Estimating the generalized sharpness for	
671	Sign Gradient Descent	24
672		
673	F.3 Results on Resnet20 and VGG11	25
674		
675	G Additional Experimental Results with Block Gradient Descent	25
676		
677	G.1 Training Details	25
678	G.2 Sensitivity of Frank-Wolfe Algorithm in Estimating the generalized sharpness for	
679	Block Gradient Descent	26
680		
681	H Additional Experimental Results with Spectral Gradient Descent	26
682		
683	H.1 Convergence When Training CNN Model	26
684	H.2 Sensitivity of Frank-Wolfe Algorithm in Estimating the Generalized Sharpness for	
685	Spectral Gradient Descent	27
686	H.3 Sensitivity of Spectral Gradient Descent to the Number of Polar Express Steps . .	27
687		
688	H.4 Quadratic Taylor Approximation of the Real Objective	27
689		
690	H.5 Results on Resnet20 and VGG11	27
691		
692	I ℓ_{∞}-descent and RMSprop	28
693		
694	A DISCUSSION ON FRANK-WOLFE ALGORITHM	
695		
696	Solving (10) reduces to the quadratic maximization problem	

$$\max_{\|\mathbf{u}\| \leq 1} \mathbf{u}^\top \mathbf{H} \mathbf{u}, \quad (23)$$

for an arbitrary norm $\|\cdot\|$ and symmetric matrix \mathbf{H} . Even in the convex case where \mathbf{H} is positive definite, problem (23) is NP-hard (Burer & Letchford, 2009) and is recognized as a fundamental challenge in global optimization (Horst et al., 2000). Consequently, without exploiting additional

structure, global optimality guarantees cannot be expected from generic first-order methods. Instead, one can provide stationarity-type guarantees or approximation bounds via relaxations (Burer & Letchford, 2009).

The Frank–Wolfe (FW) algorithm is a projection-free method that relies on a linear minimization oracle $\min_{\|\mathbf{w}\|=1} \langle \mathbf{w} - \mathbf{u}, \mathbf{H}\mathbf{u} \rangle$. For maximization problems such as (23), this oracle is applied in reverse, i.e., minimizing $-\mathbf{u}^\top \mathbf{H}\mathbf{u}$. For L -smooth functions over convex domains, which includes (23), the FW algorithm provides convergence to approximate stationary points, measured through the Frank–Wolfe gap

$$\mathcal{G}(\mathbf{u}) := \max_{\|\mathbf{w}\|\leq 1} \langle \mathbf{w} - \mathbf{u}, -\mathbf{H}\mathbf{u} \rangle,$$

where the last term comes with minus since we minimize $-\mathbf{u}^\top \mathbf{H}\mathbf{u}$. Specifically, FW identifies an iterate \mathbf{u}_K satisfying $\mathcal{G}(\mathbf{u}_K) \leq \varepsilon$ in $\mathcal{O}(1/\varepsilon^2)$ iterations, i.e., at rate $\mathcal{O}(1/\sqrt{K})$ (Lacoste-Julien, 2016). While this guarantee does not imply global optimality for (23), it provides a principled and certifiable stopping criterion. However, the solution to (23) must lie at the boundary of the unit ball in $\|\cdot\|$ norm, since the quadratic function is continuous. Therefore, in the experiments, we add a projection step. We observe that such a projection step always improved the final iterate.

As an alternative, consider the projected power iteration

$$\mathbf{u}_{k+1} = \Pi_{\|\cdot\|}(\mathbf{H}\mathbf{u}_k).$$

For the Euclidean norm, this reduces to the classical Power method, which converges to the normalized leading eigenvector provided the initialization has a nonzero component along it (Golub & Van Loan, 2013). For general norms, however, no global convergence guarantees are known: the projected iterates can stall or even cycle—for example, when they approach generalized eigenvectors, namely unit vectors \mathbf{v} that are fixed points of the linear minimization oracle, $\mathbf{v} = \operatorname{argmin}_{\|\mathbf{w}\|=1} \langle \mathbf{w} - \mathbf{v}, -\mathbf{H}\mathbf{v} \rangle$. Empirically, we found that FW provides a good estimation of (10) when a sufficient number of restarts is used.

B AN OSCILLATORY REGIME BEFORE EOS

In this appendix, we briefly elaborate on an oscillatory regime that occurs for some optimizers (including ℓ_∞ -descent and Spectral GD) *before* the algorithm reaches EoS. This stands in contrast to Euclidean GD, which generally does not oscillate before the sharpness reaches $2/\eta$ (Cohen et al., 2024).

In Figure B.1, we train a network using ℓ_∞ descent. Initially, the generalized sharpness is less than $2/\eta$, the directional smoothness is ≈ 0 , and the network’s predictions are not oscillating. Then, around step 300, even though the generalized sharpness is less than $2/\eta$, the directional smoothness starts to rise and the network’s predictions start to oscillate, which are indications that the iterates are oscillating in weight space. Finally, around step 450, the generalized sharpness and directional smoothness reach $2/\eta$ and the algorithm reaches EoS. The network’s predictions oscillate wildly.

The existence of the pre-EoS oscillatory regime is interesting, since no such regime exists for Euclidean GD.

In Figure B.2, we further explore this phenomenon. At three points during training, we switch from running ℓ_∞ descent on the real objective to running it on the quadratic Taylor approximation. We show the evolution of the network output under the resulting trajectory. Initially (left), the network output does not oscillate, indicating that the iterates are not oscillating in weight space. On the other hand, once the dynamics are in the pre-EoS oscillatory regime (middle), the network output oscillates but does not diverge. Finally, once the dynamics are at EoS (right), the network output diverges.

An interesting avenue for future work would be to understand why non-Euclidean GD starts to oscillate when it does.

756 C THE GAP BETWEEN THE GENERALIZED SHARPNESS AND $2/\eta$
757

758 Prior studies of Euclidean GD at EoS have observed that there is often a gap between the sharpness
759 and $2/\eta$; for example, in Figure 1 of Cohen et al. (2021), the sharpness can be seen to sometimes
760 exceed the critical threshold of $2/\eta$ by 150%. Similar effects can be observed in plots throughout
761 this paper for the generalized sharpness during non-Euclidean GD. We now review the prevailing
762 explanation for this phenomenon for Euclidean GD, and suggest that a similar mechanism is at play
763 for non-Euclidean GD.

764 For Euclidean GD, Cohen et al. (2025) argue that when multiple Hessian eigenvalues are near $2/\eta$, GD
765 should be conceived of as oscillating within the subspace spanned by the corresponding eigenvectors.
766 The EoS phenomenon is that for every direction \mathbf{d} in this subspace, the local time-average of the
767 directional curvature $\mathbf{d}^\top \nabla^2 \mathcal{L}(\mathbf{w}) \mathbf{d}$ is approximately equal to $2/\eta$. Concretely, if at some iteration t ,
768 one computes the top Hessian eigenvector \mathbf{d} , and then monitors the quantity $\mathbf{d}^\top \nabla^2 \mathcal{L}(\mathbf{w}_{t+j}) \mathbf{d}$ for the
769 next $j = 1, \dots, m$ iterations, then the local time-average of this quantity $\frac{1}{m} \sum_{j=1}^m \mathbf{d}^\top \nabla^2 \mathcal{L}(\mathbf{w}_{t+j}) \mathbf{d}$
770 is predicted to be approximately $2/\eta$. By contrast, if we compute the top Hessian eigenvalue anew
771 at every iteration $\{\lambda_{\max}(\nabla^2 \mathcal{L}(\mathbf{w}_t))\}$, then due to the chaotic oscillatory dynamics, we get back a
772 different vector within this subspace at every step, and because the largest Hessian eigenvector is the
773 direction with the largest curvature, there is an upward bias.

774 For an analogy, consider the random d -dimensional matrix
775

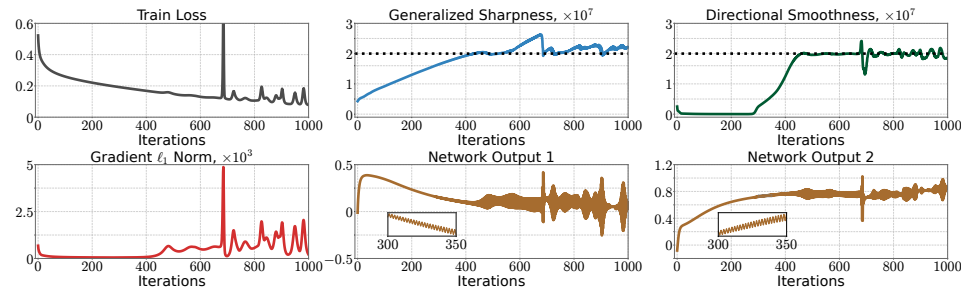
$$\mathbf{H} := \mathbf{U} \left[\frac{2}{\eta} \mathbf{I}_k + \varepsilon \text{diag}(\mathbf{z}) \right] \mathbf{U}^\top, \quad \mathbf{z} \sim \mathcal{N}(0, \mathbf{I}_k),$$

776 where $\mathbf{U} \in \mathbb{R}^{d \times k}$ has orthogonal columns and $\varepsilon > 0$ is a small number. Here, \mathbf{H} is an analogy
777 to the Hessian, the columns of \mathbf{U} are the $k \geq 2$ unstable Hessian eigenvectors, and the random
778 noise \mathbf{z} is an analogy to the chaotic oscillatory dynamics. The nonzero eigenvalues of \mathbf{H} are exactly
779 $\frac{2}{\eta} + \varepsilon \mathbf{z}$, and so the largest eigenvalue $\lambda_{\max}(\mathbf{H})$ is precisely $\frac{2}{\eta} + \varepsilon \max_{1 \leq i \leq k} z_i$. It can be shown
780 that $\mathbb{E}[\max_{1 \leq i \leq k} z_i] > 0$ provided that $k \geq 2$, and thus we have $\mathbb{E}[\lambda_{\max}(\mathbf{H})] > \frac{2}{\eta}$. On the other
781 hand, for any fixed vector $\mathbf{v} \in \text{Range}(\mathbf{U})$, we have that $\frac{\mathbb{E}[\mathbf{v}^\top \mathbf{H} \mathbf{v}]}{\|\mathbf{v}\|^2} = \frac{2}{\eta}$.
782

783 Generalizing this argument to the case of non-Euclidean GD is nontrivial, as in the non-Euclidean
784 case we do not yet know if there is an analogous concept to multiple eigenvalues being at the edge of
785 stability. Nevertheless, in Figure C.1, we empirically show that while the generalized sharpness (10)
786 hovers strictly above $2/\eta$, if we fix a timestep t_0 and compute the maximizer \mathbf{d} of the generalized
787 sharpness problem (10) at this timestep, then the quadratic form $\mathbf{d}^\top \nabla^2 \mathcal{L}(\mathbf{w}_{t_0+j}) \mathbf{d}$ computed over
788 the next $j = 1, \dots, m$ steps is much closer to $2/\eta$.
789

790 D USEFUL LEMMAS
791792 D.1 MISSING PROOFS FOR THE SPECTRAL BLOCK NORM $\ell_{\infty,2}$
793

794 First, we derive the step of Spectral GD.
795



800 Figure B.1: **An oscillatory regime before EoS.** We train a network using ℓ_∞ -descent. From steps
801 ~ 300 – 450 , the generalized sharpness is less than $2/\eta$ (so the algorithm is not yet at EoS), but
802 the directional smoothness has already started to climb from ≈ 0 towards $2/\eta$, and the network’s
803 predictions have already started to oscillate. This would not occur for Euclidean GD. This network
804 is a fully connected network trained on a subset of CIFAR-10 using MSE loss and $\eta = 1 \times 10^{-7}$.
805

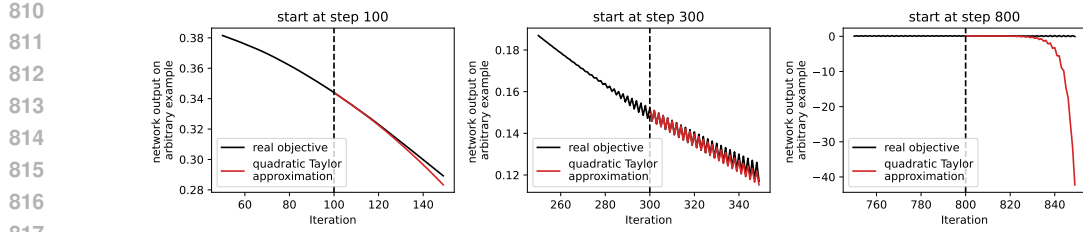


Figure B.2: **In the pre-EoS oscillatory regime, training on the quadratic Taylor approximation oscillates without diverging.** While training the network from Figure B.1, we switch from training on the real objective to training on the quadratic Taylor approximation at three points during training: at step 100 (while the optimizer is stable and non-oscillatory), at step 300 (while the optimizer is in the pre-EoS oscillatory regime), and at step 800 (when the network is at EoS). For these trajectories, we plot the network's output on an arbitrary test example. In the first case, this output evolves smoothly; in the third case, it diverges; and, interestingly, in the second case, it oscillates with sustained magnitude and without diverging.

Lemma D.1. Let $\|\mathbf{X}^\ell\|_{\mathcal{W}_\ell}$ be the norm of the ℓ -th layer and $\|\mathbf{X}\|^2 = \sum_{\ell=1}^L \|\mathbf{X}^\ell\|_{\mathcal{W}_\ell}^2$. The solution to

$$\Delta \mathbf{W}_* = \underset{\Delta \mathbf{W}}{\operatorname{argmin}} \operatorname{tr}(\Delta \mathbf{W}^\top \mathbf{G}) + \frac{1}{2\eta} \|\Delta \mathbf{W}\|^2. \quad (24)$$

is given by

$$\Delta \mathbf{W}_*^\ell = \eta \cdot \|\mathbf{G}^\ell\|_{\mathcal{W}_\ell}^* \cdot \underset{\|\mathbf{X}\|_{\mathcal{W}_\ell}=1}{\operatorname{argmin}} \operatorname{tr}(\mathbf{X}^\top \mathbf{G}^\ell) \quad (25)$$

where $\|\cdot\|_{\mathcal{W}_\ell}^*$ denotes the dual norm of $\|\cdot\|_{\mathcal{W}_\ell}$.

Proof. First, note that this problem is separable over each layer since

$$\operatorname{tr}(\Delta \mathbf{W}^\top \mathbf{G}) + \frac{1}{2\eta} \|\mathbf{W}\|^2 = \sum_{\ell=1}^L \left(\operatorname{tr}((\Delta \mathbf{W}^\ell)^\top \mathbf{G}^\ell) + \frac{1}{2\eta} \|\Delta \mathbf{W}^\ell\|_{\mathcal{W}_\ell}^2 \right).$$

Thus, we can solve over each layer separately. Changing coordinates with $\Delta \mathbf{W}^\ell = c \mathbf{X}$ where $\|\mathbf{X}\|_{\mathcal{W}_\ell} = 1$ and $c \geq 0$ we have that

$$\begin{aligned} \min_{\Delta \mathbf{W}^\ell} \operatorname{tr}((\Delta \mathbf{W}^\ell)^\top \mathbf{G}^\ell) + \frac{1}{2\eta} \|\Delta \mathbf{W}^\ell\|_{\mathcal{W}_\ell}^2 &= \min_{c \geq 0} c \min_{\|\mathbf{X}\|_{\mathcal{W}_\ell}=1} \operatorname{tr}(\mathbf{X}^\top \mathbf{G}^\ell) + \frac{1}{2\eta} c^2 \\ &= \min_{c \geq 0} -c \|\mathbf{G}^\ell\|_{\mathcal{W}_\ell}^* + \frac{1}{2\eta} c^2. \end{aligned}$$

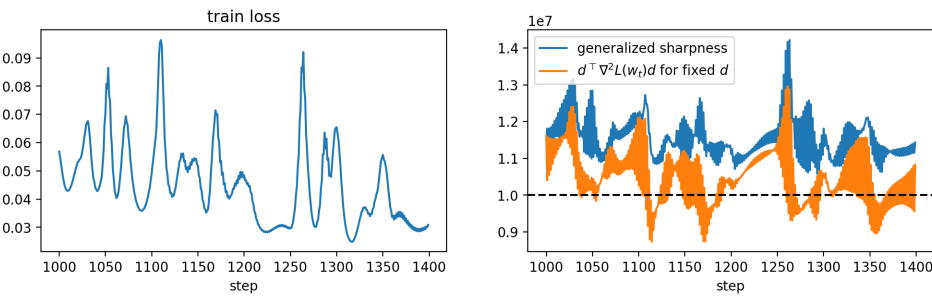


Figure C.1: For a stretch of training, we plot both the (estimated) generalized sharpness $\max_{\|\mathbf{d}\| \leq 1} \mathbf{d}^\top \nabla^2 \mathcal{L}(\mathbf{w}_t) \mathbf{d}$ (blue), as well as the quadratic form $\mathbf{d}_*^\top \nabla^2 \mathcal{L}(\mathbf{w}_t) \mathbf{d}_*$ where $\mathbf{d}_* \in \operatorname{argmax}_{\|\mathbf{d}\| \leq 1} \mathbf{d}^\top \nabla^2 \mathcal{L}(\mathbf{w}_t)$ is the maximizing direction at step $t_0 = 1000$. While the first quantity is consistently larger than $2/\eta$, the second is much closer to $2/\eta$. This is a fully-connected network trained on a subset of CIFAR-10 using MSE loss and ℓ_∞ descent with $\eta = 2e-7$.

864 Here, we use the fact that $\underset{\mathbf{X}}{\operatorname{argmin}} \operatorname{tr}(\mathbf{X}^\top \mathbf{G}^\ell) = -(\mathbf{G}^\ell)^*$ is the dual matrix of \mathbf{G}^ℓ . Finally solving
 865 in $c \geq 0$ gives $c = \eta \cdot \|\mathbf{G}_\ell\|_{\mathcal{W}_\ell}^*$.
 866

□

868
 869 If we use the infinity norm over layers instead of the Euclidean one, we get the following re-
 870 sult.
 871

872 **Lemma D.2.** The solution to

$$873 \Delta \mathbf{W}_* = \underset{\Delta \mathbf{W}}{\operatorname{argmin}} \operatorname{tr}(\Delta \mathbf{W}^\top \mathbf{G}_t) + \frac{1}{2\eta} \max_{\ell \in [L]} \|\Delta \mathbf{W}^\ell\|_{\mathcal{W}_\ell}^2. \quad (26)$$

874 is given by
 875

$$876 \Delta \mathbf{W}_*^\ell = \eta \gamma \cdot \underset{\|\mathbf{X}\|_{\mathcal{W}_\ell} = 1}{\operatorname{argmin}} \operatorname{tr}(\mathbf{X}^\top \mathbf{G}_t^\ell) \quad (27)$$

877 where $\gamma := \sum_{\ell=1}^L \|\mathbf{G}_t^\ell\|_{\mathcal{W}_\ell}^*$ and $\|\cdot\|_{\mathcal{W}_\ell}^*$ denotes the dual norm of $\|\cdot\|_{\mathcal{W}_\ell}$.
 878

879 **Remark D.3.** If $\|\cdot\|_{\mathcal{W}_\ell} = \|\cdot\|_2$ for all $\ell \in [L]$, then $\Delta \mathbf{W}^\ell = \eta \gamma \mathbf{U}_t^\ell \mathbf{V}_t^\ell$ where $\mathbf{G}_t^\ell = \mathbf{U}_t^\ell \Sigma_t^\ell \mathbf{V}_t^\ell$ is
 880 the reduced SVD decomposition. Moreover, $\gamma = \sum_{\ell=1}^L \|\mathbf{G}_t^\ell\|_*$ is the sum of nuclear norms over
 881 the layers. See the proof in (Bernstein & Newhouse, 2024).
 882

883 *Proof.* The problem that we want to solve is
 884

$$885 \min_{\Delta \mathbf{W}} \sum_{\ell=1}^L \operatorname{tr}((\Delta \mathbf{W}^\ell)^\top \mathbf{G}_t^\ell) + \frac{1}{2\eta} \max_{\ell \in [L]} \|\Delta \mathbf{W}^\ell\|_{\mathcal{W}_\ell}^2;$$

886 Let $\mathcal{S} := \{\Delta \mathbf{W} \mid \|\Delta \mathbf{W}^\ell\|_{\mathcal{W}_\ell} \leq t \forall \ell \in [L]\}$. We can rewrite this problem as
 887

$$888 \min_{t \geq 0} \min_{\Delta \mathbf{W} \in \mathcal{S}} \left[\sum_{\ell=1}^L \operatorname{tr}((\Delta \mathbf{W}^\ell)^\top \mathbf{G}_t^\ell) + \frac{1}{2\eta} \|\Delta \mathbf{W}^\ell\|_{\mathcal{W}_\ell}^2 \right] = \min_{t \geq 0} \min_{\Delta \mathbf{W} \in \mathcal{S}} \left[\sum_{\ell=1}^L \operatorname{tr}((\Delta \mathbf{W}^\ell)^\top \mathbf{G}_t^\ell) + \frac{t^2}{2\eta} \right]$$

$$889 = \min_{t \geq 0} \left[\sum_{\ell=1}^L \min_{\|\Delta \mathbf{W}^\ell\|_{\mathcal{W}_\ell} \leq t} \operatorname{tr}((\Delta \mathbf{W}^\ell)^\top \mathbf{G}_t^\ell) + \frac{t^2}{2\eta} \right] = \min_{t \geq 0} \left[\sum_{\ell=1}^L -t \max_{\|\Delta \mathbf{W}^\ell\|_{\mathcal{W}_\ell} \leq 1} \operatorname{tr}((\Delta \mathbf{W}^\ell)^\top \mathbf{G}_t^\ell) + \frac{t^2}{2\eta} \right]$$

$$890 = \min_{t \geq 0} \left[\sum_{\ell=1}^L -t \|\mathbf{G}_t^\ell\|_{\mathcal{W}_\ell}^* + \frac{t^2}{2\eta} \right].$$

901 Now it is a quadratic problem in t . The minimizer t_* is given by
 902

$$903 t_* := \eta \sum_{\ell=1}^L \|\mathbf{G}_t^\ell\|_{\mathcal{W}_\ell}^*.$$

904 Therefore, the final solution is given by
 905

$$906 \Delta \mathbf{W}^\ell = \eta \left(\sum_{\ell=1}^L \|\mathbf{G}_t^\ell\|_{\mathcal{W}_\ell}^* \right) \underset{\|\mathbf{X}\|_{\mathcal{W}_\ell} \leq 1}{\operatorname{argmin}} \operatorname{tr}(\mathbf{X}^\top \mathbf{G}_t^\ell).$$

□

907
 908 **Lemma D.4.** Let $\|\cdot\|$ be the spectral block norm $\|\cdot\|_{2 \rightarrow 2}$. Then the iterates of the FW to approxi-
 909 mate (19) are given by
 910

$$911 \mathbf{U}_k^\ell \mathbf{V}_k^\ell = \operatorname{polar}(\nabla_{\mathbf{W}^\ell} F(\mathbf{D}_t)), \quad \mathbf{D}_{k+1}^\ell = (1 - \gamma_k) \mathbf{D}_k + \gamma_k \mathbf{U}_k^\ell \mathbf{V}_k^\ell,$$

918 where $\text{polar}(\cdot)$ is the polar decomposition of a matrix, $\gamma_k = \frac{2}{2+k}$

920

921 *Proof.* We consider the Frank-Wolfe method for finding an approximate solution. For shortness,
922 let $\mathbf{H} := \nabla^2 \mathcal{L}(\mathbf{W}_t)$, and note that the objective $F(\mathbf{D}) := \langle \mathbf{D}, \mathbf{H}[\mathbf{D}] \rangle$ is a quadratic form, whose
923 gradient is given by

$$924 \quad \nabla F(\mathbf{D}) = 2\mathbf{H}[\mathbf{D}].$$

925 To compute a step of the Frank-Wolfe method, we need to solve

$$927 \quad \underset{\mathbf{D}}{\text{argmin}} \quad \langle \nabla F(\mathbf{D}_k), \mathbf{D} \rangle \quad \text{subject to } \|\mathbf{D}^\ell\|_2 \leq 1, \quad \text{for } \ell = 1, \dots, L.$$

929 Clearly, this problem is separable over layers and is thus equivalent to solving (Bernstein & New-
930 house, 2024)

$$931 \quad \mathbf{U}_k^\ell \mathbf{V}_k^\ell = \underset{\mathbf{D}^\ell}{\text{argmin}} \quad \langle \nabla_{\mathbf{W}^\ell} F(\mathbf{D}_k), \mathbf{D}^\ell \rangle \quad \text{subject to } \|\mathbf{D}^\ell\|_2 \leq 1,$$

934 where $\nabla_{\mathbf{W}^\ell} F(\mathbf{D}_k)$ is the directional derivative of the gradient of the ℓ -th layer given by

$$935 \quad \nabla_{\mathbf{W}^\ell} F(\mathbf{D}_k) = \frac{d}{d\epsilon} \nabla_{\mathbf{W}^\ell} \mathcal{L}(\mathbf{D}_k^1, \dots, \mathbf{D}_k^\ell + \epsilon \mathbf{D}^\ell, \dots, \mathbf{D}_k^L) \Big|_{\epsilon=0}$$

938 and where $\mathbf{U}_k^\ell \mathbf{\Sigma}_k^\ell \mathbf{V}_k^\ell = \nabla_{\mathbf{W}^\ell} F(\mathbf{D}_k)$. The matrix $\mathbf{U}_k^\ell \mathbf{V}_k^\ell$ is also known as the polar factor of
939 $\nabla_{\mathbf{W}^\ell} F(\mathbf{D}_k)$. The resulting Frank-Wolfe method is thus given by

$$941 \quad \mathbf{U}_k^\ell \mathbf{V}_k^\ell = \text{polar}(\nabla_{\mathbf{W}^\ell} F(\mathbf{D}_k)), \quad \mathbf{D}_{k+1}^\ell = (1 - \gamma_k) \mathbf{D}_k^\ell + \gamma_k \mathbf{U}_k^\ell \mathbf{V}_k^\ell,$$

943 where $\gamma_k = \frac{2}{k+2}$. □

944

945 D.2 MISSING PROOFS FOR THE BLOCK $\ell_{1,2}$ NORM

946

947 **Lemma D.5.** The solution to the problem

$$948 \quad \Delta \mathbf{w}_* = \underset{\mathbf{w}}{\text{argmin}} \quad \langle \Delta \mathbf{w}, \mathbf{g}_t \rangle + \frac{1}{2\eta} \|\Delta \mathbf{w}\|_{1,2}^2$$

950 can be written as

$$951 \quad \Delta \mathbf{w}_*^\ell = \begin{cases} 0 & \text{if } \mathbf{g}_t = 0, \\ 0 & \text{if } \mathbf{g}_t \neq 0 \text{ and } \ell \notin J, \\ -\frac{\eta}{|J|} \mathbf{g}_t^\ell & \ell \in J, \end{cases}$$

955 where $J := \{\ell \in [L] \mid \|\mathbf{g}_t^\ell\|_2 = \max_{j \in [L]} \|\mathbf{g}_t^j\|_2\}$.

957

958 **Remark D.6.** In the case when J is a singleton, we obtain Block CD

$$959 \quad \mathbf{w}_{t+1}^\ell = \begin{cases} \mathbf{w}_t^\ell - \eta \mathbf{g}_t^\ell & \text{if } \ell = \ell_{\max}, \\ \mathbf{w}_t^\ell & \text{otherwise,} \end{cases}$$

960 where $\ell_{\max} = \underset{\ell \in [L]}{\text{argmax}} \|\mathbf{g}_t^\ell\|_2$.

964

965 **Remark D.7.** In the case when $L = d$, we obtain vanilla coordinate descent (CD)

$$966 \quad \mathbf{w}_{t+1}^j = \begin{cases} \mathbf{w}_t^{j_{\max}} - \eta \mathbf{g}_t^{j_{\max}} & \text{if } j = j_{\max} \\ \mathbf{w}_t^j & \text{otherwise,} \end{cases}$$

967 where $j_{\max} = \underset{j \in [d]}{\text{argmax}} |\mathbf{g}_t^j|$.

972 *Proof.* We need to find a solution to the problem
 973

$$974 \min_{\Delta \mathbf{w}} \langle \Delta \mathbf{w}, \mathbf{g}_t \rangle + \frac{1}{2\eta} \left(\sum_{\ell=1}^L \|\Delta \mathbf{w}^\ell\|_2 \right)^2 = \min_{\Delta \mathbf{w}} \sum_{\ell=1}^L \langle \Delta \mathbf{w}^\ell, \mathbf{g}_t^\ell \rangle + \frac{1}{2\eta} \left(\sum_{\ell=1}^L \|\Delta \mathbf{w}^\ell\|_2 \right)^2$$

975 Let $\Delta \mathbf{w}_*$ be the solution to the problem. Therefore,
 976

$$977 \begin{aligned} 0 &\in \mathbf{g}_t + \frac{1}{\eta} \left(\sum_{\ell=1}^L \|\Delta \mathbf{w}_*^\ell\|_2 \right) \partial \left(\sum_{\ell=1}^L \|\Delta \mathbf{w}_*^\ell\|_2 \right) \\ 978 &= \mathbf{g}_t + \frac{1}{\eta} \left(\sum_{\ell=1}^L \|\Delta \mathbf{w}_*^\ell\|_2 \right) (\partial \|\Delta \mathbf{w}_*^1\|_2^\top, \dots, \partial \|\Delta \mathbf{w}_*^L\|_2^\top)^\top. \end{aligned} \quad (28)$$

979 Let $\chi = \sum_{\ell=1}^L \|\Delta \mathbf{w}_*^\ell\|_2$. Note that
 980

$$981 \partial \|\mathbf{x}\| = \begin{cases} \frac{\mathbf{x}}{\|\mathbf{x}\|_2} & \text{if } \mathbf{x} \neq 0, \\ \{\mathbf{y} \mid \|\mathbf{y}\|_2 \leq 1\} & \text{otherwise} \end{cases}.$$

982 Therefore, we should satisfy the following L equalities
 983

$$984 \mathbf{g}_t^\ell = \frac{\chi}{\eta} \partial \|\Delta \mathbf{w}_*^\ell\|_2, \quad \text{and} \quad \|\mathbf{g}_t^\ell\|_2 = \frac{\chi}{\eta} \|\partial \|\Delta \mathbf{w}_*^\ell\|_2\| \leq \frac{\chi}{\eta}. \quad (29)$$

985 This implies that each block of \mathbf{g}_t has a norm at most χ/η , and whenever some block ℓ satisfies
 986 $\partial \|\Delta \mathbf{w}_*^\ell\|_2 = \frac{\Delta \mathbf{w}_*^\ell}{\|\Delta \mathbf{w}_*^\ell\|_2}$, then the corresponding block $\|\mathbf{g}_t^\ell\|_2 = \frac{\chi}{\eta}$.
 987

988 If $\|\mathbf{g}_t^\ell\|_2 = 0$ for all $\ell \in [L]$, i.e., $\mathbf{g}_t = 0$, then for all $\Delta \mathbf{w}_*^\ell = 0$.
 989

990 Now let us assume that there is at least one block $\ell \in [L]$ such that $\|\mathbf{g}_t^\ell\|_2 \neq 0$. Let $J := \{\ell \in [L] \mid \|\mathbf{g}_t^\ell\|_2 = \max_{j \in [L]} \|\mathbf{g}_t^j\|_2\} \neq \emptyset$. Then, for all blocks $\ell \in J$ we have $\|\mathbf{g}_t^\ell\|_2 = \frac{\chi}{\eta}$. Indeed, if it is not the case, i.e., if for all $\ell \in [L]$ we have $\|\mathbf{g}_t^\ell\|_2 < \frac{\chi}{\eta}$, then $\Delta \mathbf{w}_* = 0$ and we obtain a contradiction to (28) since $\mathbf{g}_t \neq 0$.
 991

992 We summarize that for any block $\ell \notin J$ such that $\|\mathbf{g}_t^\ell\|_2 < \frac{\chi}{\eta}$ we obtain $\Delta \mathbf{w}_*^\ell = 0$. In the opposite
 993 case for $\ell \in J$, we have that
 994

$$995 \|\mathbf{g}_t^\ell\|_2 = \max_{j \in [L]} \|\mathbf{g}_t^j\|_2 = \frac{\chi}{\eta} \Rightarrow \chi = \sum_{\ell \in J} \|\Delta \mathbf{w}_*^\ell\|_2 = |J| \max_{\ell \in J} \|\Delta \mathbf{w}_*^\ell\| = \eta \max_{\ell \in [L]} \|\mathbf{g}_t^\ell\|,$$

996 and from (29) we obtain $\Delta \mathbf{w}_*^\ell = -\frac{\eta \max_{j \in [L]} \|\mathbf{g}_t^j\|_2}{|J|} \frac{\mathbf{g}_t^\ell}{\|\mathbf{g}_t^\ell\|_2} = -\frac{\eta}{|J|} \mathbf{g}_t^\ell$ for $\ell \in J$. This concludes the
 997 proof. \square
 998

1000 **Lemma D.8.** Let $\|\cdot\|$ be the block $\ell_{1,2}$ norm. Assume that the Hessian $\nabla^2 \mathcal{L}(\mathbf{w}_t)$ is positive semi-definite. Then the generalized sharpness (16) is given by
 1001

$$1002 S^{\|\cdot\|_{1,2}}(\mathbf{w}_t) = \max_{\ell \in [L]} \lambda_{\max}(\nabla_{\mathbf{w}^\ell}^2 \mathcal{L}(\mathbf{w}_t)).$$

1003 *Proof.* If $\mathbf{H} = \nabla^2 \mathcal{L}(\mathbf{w}_t)$ is positive semidefinite, then the function $f(\mathbf{d}) = \langle \mathbf{d}, \mathbf{H} \mathbf{d} \rangle$ is convex.
 1004 Our goal is to find the maximum of this quadratic convex function over a $\ell_{1,2}$ -norm unit ball. It
 1005 attains the maximum at the border, i.e., $\|\mathbf{d}\|_{1,2} = 1$. Any point \mathbf{y} at the border of the $\ell_{1,2}$ unit norm
 1006 can be expressed as
 1007

$$1008 \mathbf{y} = (\alpha_1 \mathbf{d}^1, \dots, \alpha_L \mathbf{d}^L) \quad \text{where} \quad \|\mathbf{d}^\ell\|_2 = 1 \quad \forall \ell \in [L] \quad \text{and} \quad \sum_{\ell=1}^L \alpha_\ell = 1.$$

1009 Let $\mathbf{y}_1 = (\mathbf{d}^1, 0, \dots, 0)$, $\mathbf{y}_2 = (0, \mathbf{d}^2, \dots, 0)$, \dots , $\mathbf{y}_L = (0, 0, \dots, \mathbf{d}^L)$, $\|\mathbf{d}^\ell\|_2 = 1$ for all $\ell \in [L]$. Then $\mathbf{y} = \sum_{\ell=1}^L \alpha_\ell \mathbf{y}_\ell$. Since f is convex, then $f(\mathbf{y}) \leq \sum_{\ell=1}^L \alpha_\ell f(\mathbf{y}_\ell) \leq \max_{\ell \in [L]} f(\mathbf{y}_\ell)$.
 1010 Therefore, our problem reduces to
 1011

$$1012 \max_{\ell \in [L]} \max_{\|\mathbf{d}^\ell\|_2=1} \langle \mathbf{d}^\ell, \nabla_{\mathbf{w}^\ell}^2 \mathcal{L}(\mathbf{w}_t) \mathbf{d}^\ell \rangle = \max_{\ell \in [L]} \lambda_{\max}(\nabla_{\mathbf{w}^\ell}^2 \mathcal{L}(\mathbf{w}_t)), \quad (30)$$

1026 where $\nabla_{\mathbf{w}^\ell}^2 \mathcal{L}(\mathbf{w}_t)$ is the ℓ -th diagonal block of the Hessian. In the special case of $L = d$, we have
 1027 the sharpness measure
 1028

$$1029 \max_{\mathbf{d}} \frac{\mathbf{d}^\top \nabla^2 \mathcal{L}(\mathbf{w}_t) \mathbf{d}}{\|\mathbf{d}\|_1^2} = \max_j |\nabla^2 \mathcal{L}(\mathbf{w}_t)_{jj}|.$$

□

1034 **Lemma D.9.** Let $\|\cdot\|$ be the block $\ell_{1,2}$ norm. Then the iterates of the FW to approximate (16) are
 1035 given by

$$1036 \mathbf{v}_k = \frac{(\nabla^2 \mathcal{L}(\mathbf{w}_t) \mathbf{d}_k)_\ell}{\|(\nabla^2 \mathcal{L}(\mathbf{w}_t) \mathbf{d}_k)_\ell\|_2}, \quad \mathbf{d}_{k+1} = (1 - \gamma_k) \mathbf{d}_k + \gamma_k \mathbf{v}_k,$$

1038 where $(\nabla^2 \mathcal{L}(\mathbf{w}_t) \mathbf{d}_k)_\ell$ is the ℓ -th block of the vector $\nabla^2 \mathcal{L}(\mathbf{w}_t) \mathbf{d}_k$, and $\gamma_k = \frac{2}{2+k}$.
 1039

1040 *Proof.* We consider the Frank-Wolfe method for finding an approximate solution. For shortness, let
 1041 $\mathbf{H} := \nabla^2 \mathcal{L}(\mathbf{w}_t)$, and note that the objective $F(\mathbf{d}) := \mathbf{d}^\top \mathbf{H} \mathbf{d}$ is a quadratic form, whose gradient is
 1042 given by $\nabla F(\mathbf{d}) = 2\mathbf{H}\mathbf{d}$. To compute a step of the Frank-Wolfe method, we need to solve
 1043

$$1044 \operatorname{argmin}_{\mathbf{d}} \langle \nabla F(\mathbf{d}_k), \mathbf{d} \rangle \quad \text{subject to } \|\mathbf{d}\|_{1,2} \leq 1.$$

1045 The solution to this is given by the dual norm and the dual gradient

$$1046 \min_{\|\mathbf{d}\|_{1,2} \leq 1} \langle \nabla F(\mathbf{d}_k), \mathbf{d} \rangle = \|\nabla F(\mathbf{d}_k)\|_{\infty,2} = \max_{\ell \in [L]} \|\nabla_{\mathbf{d}^\ell} F(\mathbf{d}_k)\|_2.$$

1047 This is true, since

$$1048 \begin{aligned} \langle \nabla F(\mathbf{d}_k), \mathbf{d} \rangle &= \sum_{\ell=1}^L \langle \nabla_{\mathbf{d}^\ell} F(\mathbf{d}_k), \mathbf{d}^\ell \rangle \leq \sum_{\ell=1}^L \|\nabla_{\mathbf{d}^\ell} F(\mathbf{d}_k)\|_2 \cdot \|\mathbf{d}^\ell\|_2 \\ 1049 &\leq \max_{\ell \in [L]} \|\nabla_{\mathbf{d}^\ell} F(\mathbf{d}_k)\|_2 \cdot \sum_{\ell=1}^L \|\mathbf{d}^\ell\|_2 = \max_{\ell \in [L]} \|\nabla_{\mathbf{d}^\ell} F(\mathbf{d}_k)\|_2. \end{aligned} \quad (31)$$

1050 The maximizer is obtained by concentrating all mass on any group $\ell \in \{\ell : \|\nabla_{\mathbf{d}^\ell} F(\mathbf{d}_k)\|_2 = \max_{i \in [L]} \|\nabla_{\mathbf{d}^i} F(\mathbf{d}_k)\|_2\}$, namely,
 1051

$$1052 \mathbf{d}_*^\ell = \begin{cases} \frac{\nabla_{\mathbf{d}^\ell} F(\mathbf{d}_k)}{\|\nabla_{\mathbf{d}^\ell} F(\mathbf{d}_k)\|_2}, & \ell \in \{j : \|\nabla_{\mathbf{d}^j} F(\mathbf{d}_k)\|_2 = \max_{i \in [L]} \|\nabla_{\mathbf{d}^i} F(\mathbf{d}_k)\|_2\} \\ 0, & \text{otherwise.} \end{cases}$$

□

1064 E NON-EUCLIDEAN GRADIENT DESCENT ON QUADRATICS

1065 To prove convergence of Non-Euclidean GD for the case of a sufficiently small step size, (Theorem
 1066 5.1) we follow standard arguments of smoothness and strong convexity. The following definitions
 1067 of smoothness and strong convexity are standard generalizations from the Euclidean norm to an
 1068 arbitrary norm.
 1069

1070 **Definition E.1.** We say that $\mathcal{L} : \mathbb{R}^d \rightarrow \mathbb{R}$ is $(L, \|\cdot\|)$ -smooth if

$$1071 \|\nabla \mathcal{L}(\mathbf{w}) - \nabla \mathcal{L}(\mathbf{v})\|_* \leq L \|\mathbf{w} - \mathbf{v}\| \quad (32)$$

1072 for all $\mathbf{w}, \mathbf{v} \in \mathbb{R}^d$.
 1073

1074 **Definition E.2.** We say that $\mathcal{L} : \mathbb{R}^d \rightarrow \mathbb{R}$ is $(\mu, \|\cdot\|)$ -strongly convex if

$$1075 \mathcal{L}(\mathbf{v}) \geq \mathcal{L}(\mathbf{w}) + \langle \nabla \mathcal{L}(\mathbf{w}), \mathbf{v} - \mathbf{w} \rangle + \frac{\mu}{2} \|\mathbf{v} - \mathbf{w}\|^2 \quad (33)$$

1080 for all $\mathbf{w}, \mathbf{v} \in \mathbb{R}^d$.
 1081

1082 The following lemmas show that our quadratic $\mathcal{L}(\mathbf{w}) = \frac{1}{2}\mathbf{w}^\top \mathbf{H}\mathbf{w}$ is smooth and strongly convex.
 1083

1084 **Lemma E.3.** The objective $\mathcal{L}(\mathbf{w}) = \frac{1}{2}\mathbf{w}^\top \mathbf{H}\mathbf{w}$ is $(L, \|\cdot\|)$ -smooth with $L = \sup_{\|\mathbf{z}\|=1} \mathbf{z}^\top \mathbf{H}\mathbf{z}$.
 1085

1086 *Proof.* For any $\mathbf{w}, \mathbf{v} \in \mathbb{R}^d$, denote $\mathbf{d} = (\mathbf{w} - \mathbf{v})/\|\mathbf{w} - \mathbf{v}\|$. Then
 1087

$$\frac{\|\nabla \mathcal{L}(\mathbf{w}) - \nabla \mathcal{L}(\mathbf{v})\|_*}{\|\mathbf{w} - \mathbf{v}\|} = \frac{\|\mathbf{H}\mathbf{w} - \mathbf{H}\mathbf{v}\|_*}{\|\mathbf{w} - \mathbf{v}\|} = \|\mathbf{H}\mathbf{d}\|_* = \sup_{\|\mathbf{u}_1\|=1} \mathbf{u}_1^\top \mathbf{H}\mathbf{d} \leq \sup_{\|\mathbf{u}_1\|=\|\mathbf{u}_2\|=1} \mathbf{u}_1^\top \mathbf{H}\mathbf{u}_2, \quad (34)$$

1092 where in the third equality we used the definition of dual norm. Next we will prove that
 1093

$$\sup_{\|\mathbf{u}_1\|=\|\mathbf{u}_2\|=1} \mathbf{u}_1^\top \mathbf{H}\mathbf{u}_2 = \sup_{\|\mathbf{z}\|=1} \mathbf{z}^\top \mathbf{H}\mathbf{z}.$$

1096 The (\geq) direction is immediate since
 1097

$$\sup_{\|\mathbf{u}_1\|=\|\mathbf{u}_2\|=1} \mathbf{u}_1^\top \mathbf{H}\mathbf{u}_2 \geq \sup_{\|\mathbf{z}\|=1} \mathbf{z}^\top \mathbf{H}\mathbf{z}. \quad (35)$$

1100 To show the other direction, let

$$(\mathbf{u}_1^*, \mathbf{u}_2^*) \in \underset{\|\mathbf{u}_1\|=\|\mathbf{u}_2\|=1}{\operatorname{argmax}} \mathbf{u}_1^\top \mathbf{H}\mathbf{u}_2, \quad (36)$$

1103 and

$$\mathbf{z}^* \in \underset{\|\mathbf{z}\|=1}{\operatorname{argmax}} \mathbf{z}^\top \mathbf{H}\mathbf{z}. \quad (37)$$

1104 Note that these argmax operations make sense, since we are considering the maximum of continuous
 1105 functions on compact domains, which always achieve their supremum. Then
 1106

$$\begin{aligned} (\mathbf{u}_1^* - \mathbf{u}_2^*)^\top \mathbf{H}(\mathbf{u}_1^* - \mathbf{u}_2^*) &\geq 0 \\ (\mathbf{u}_1^*)^\top \mathbf{H}\mathbf{u}_1^* - 2(\mathbf{u}_1^*)^\top \mathbf{H}\mathbf{u}_2^* + (\mathbf{u}_2^*)^\top \mathbf{H}\mathbf{u}_2^* &\geq 0 \\ (\mathbf{u}_1^*)^\top \mathbf{H}\mathbf{u}_1^* + (\mathbf{u}_2^*)^\top \mathbf{H}\mathbf{u}_2^* &\geq 2(\mathbf{u}_1^*)^\top \mathbf{H}\mathbf{u}_2^* \\ 2(\mathbf{z}^*)^\top \mathbf{H}\mathbf{z}^* &\geq 2(\mathbf{u}_1^*)^\top \mathbf{H}\mathbf{u}_2^* \\ (\mathbf{z}^*)^\top \mathbf{H}\mathbf{z}^* &\geq (\mathbf{u}_1^*)^\top \mathbf{H}\mathbf{u}_2^*, \end{aligned}$$

1107 where the first inequality uses that \mathbf{H} is PSD, the second inequality uses that \mathbf{H} is symmetric, and
 1108 the fourth inequality uses $(\mathbf{u}_1^*)^\top \mathbf{H}\mathbf{u}_1^* \leq (\mathbf{z}^*)^\top \mathbf{H}\mathbf{z}^*$ and $(\mathbf{u}_2^*)^\top \mathbf{H}\mathbf{u}_2^* \leq (\mathbf{z}^*)^\top \mathbf{H}\mathbf{z}^*$. This proves
 1109 the (\leq) direction, and proves the claim. Then Equation (34) becomes
 1110

$$\frac{\|\nabla \mathcal{L}(\mathbf{w}) - \nabla \mathcal{L}(\mathbf{v})\|_*}{\|\mathbf{w} - \mathbf{v}\|} \leq \sup_{\|\mathbf{z}\|=1} \mathbf{z}^\top \mathbf{H}\mathbf{z}, \quad (38)$$

1111 or

$$\|\nabla \mathcal{L}(\mathbf{w}) - \nabla \mathcal{L}(\mathbf{v})\|_* \leq \left(\sup_{\|\mathbf{z}\|=1} \mathbf{z}^\top \mathbf{H}\mathbf{z} \right) \|\mathbf{w} - \mathbf{v}\|. \quad (39)$$

1112 \square
 1113

1114 **Lemma E.4.** The objective $\mathcal{L}(\mathbf{w}) = \frac{1}{2}\mathbf{w}^\top \mathbf{H}\mathbf{w}$ is $(\mu, \|\cdot\|)$ -strongly convex with $\mu = \inf_{\|\mathbf{v}\|=1} \mathbf{v}^\top \mathbf{H}\mathbf{v}$.
 1115

1116 *Proof.* The strong convexity property
 1117

$$\mathcal{L}(\mathbf{v}) \geq \mathcal{L}(\mathbf{w}) + \langle \nabla \mathcal{L}(\mathbf{w}), \mathbf{v} - \mathbf{w} \rangle + \frac{\mu}{2} \|\mathbf{v} - \mathbf{w}\|^2 \quad (40)$$

1134 for our particular \mathcal{L} is equivalent to each of the following statements:
1135

$$1136 \quad \frac{1}{2}\mathbf{v}^\top \mathbf{H}\mathbf{v} \geq \frac{1}{2}\mathbf{w}^\top \mathbf{H}\mathbf{w} + (\mathbf{v} - \mathbf{w})^\top \mathbf{H}\mathbf{w} + \frac{\mu}{2}\|\mathbf{v} - \mathbf{w}\|^2 \quad (41)$$

$$1138 \quad \frac{1}{2}\mathbf{v}^\top \mathbf{H}\mathbf{v} - \mathbf{v}^\top \mathbf{H}\mathbf{w} + \frac{1}{2}\mathbf{w}^\top \mathbf{H}\mathbf{w} \geq \frac{\mu}{2}\|\mathbf{v} - \mathbf{w}\|^2 \quad (42)$$

$$1140 \quad (\mathbf{v} - \mathbf{w})^\top \mathbf{H}(\mathbf{v} - \mathbf{w}) \geq \mu\|\mathbf{v} - \mathbf{w}\|^2 \quad (43)$$

$$1142 \quad \left(\frac{\mathbf{v} - \mathbf{w}}{\|\mathbf{v} - \mathbf{w}\|} \right)^\top \mathbf{H} \frac{\mathbf{v} - \mathbf{w}}{\|\mathbf{v} - \mathbf{w}\|} \geq \mu, \quad (44)$$

1144 which is satisfied by $\mu = \inf_{\|\mathbf{v}\|=1} \mathbf{v}^\top \mathbf{H}\mathbf{v}$. \square
1145

1147 **Theorem 5.1.** Let $\mathcal{L}(\mathbf{w}) := \frac{1}{2}\mathbf{w}^\top \mathbf{H}\mathbf{w}$ for some $\mathbf{H} \succ 0$. For some norm $\|\cdot\|$, define the general-
1148 ized sharpness $S = S^{\|\cdot\|} := \max_{\|\mathbf{d}\| \leq 1} \mathbf{d}^\top \mathbf{H}\mathbf{d}$. If we run non-Euclidean GD (Def. 1.1) on \mathcal{L} with
1149 any step-size $\eta < 2/S$, it will converge at a linear rate starting from any initial point \mathbf{w}_0 .
1150

1152 *Proof.* To show convergence, we prove a generalization of the Polyak-Łojasiewicz (PL) property,
1153 then follow the standard analysis of gradient descent for smooth and PL functions.

1154 Lemma E.4 implies that \mathcal{L} is μ -strongly convex with $\mu = \inf_{\|\mathbf{v}\|=1} \mathbf{v}^\top \mathbf{H}\mathbf{v}$. We also know that
1155 $\mathcal{L}(\mathbf{w}) \geq \mathcal{L}_* := 0$, and that this minimum is achieved at $\mathbf{w}_* = \mathbf{0}$. So we apply (33) with $\mathbf{v} = \mathbf{w}_*$
1156 and any \mathbf{w} :

$$1158 \quad \mathcal{L}_* \geq \mathcal{L}(\mathbf{w}) + \langle \nabla \mathcal{L}(\mathbf{w}), \mathbf{w}_* - \mathbf{w} \rangle + \frac{\mu}{2}\|\mathbf{w}_* - \mathbf{w}\|^2 \quad (45)$$

$$1160 \quad \geq \inf_{\mathbf{v}} \left\{ \mathcal{L}(\mathbf{w}) + \langle \nabla \mathcal{L}(\mathbf{w}), \mathbf{v} - \mathbf{w} \rangle + \frac{\mu}{2}\|\mathbf{v} - \mathbf{w}\|^2 \right\}. \quad (46)$$

1162 From (1), we know the inf above is minimized when $\mathbf{v} = \mathbf{w} - 1/\mu\|\nabla \mathcal{L}(\mathbf{w})\|_* (\nabla \mathcal{L}(\mathbf{w}))_*$. We also
1163 know that $\mathcal{L}(\mathbf{w}) \geq \mathcal{L}_* := 0$ for all \mathbf{w} . So

$$1165 \quad \mathcal{L}_* \geq \mathcal{L}(\mathbf{w}) - \frac{1}{\mu}\|\nabla \mathcal{L}(\mathbf{w})\|_* \langle \nabla \mathcal{L}(\mathbf{w}), (\nabla \mathcal{L}(\mathbf{w}))_* \rangle + \frac{1}{2\mu}\|\nabla \mathcal{L}(\mathbf{w})\|_*^2 \|(\nabla \mathcal{L}(\mathbf{w}))_*\|^2 \quad (47)$$

$$1167 \quad = \mathcal{L}(\mathbf{w}) - \frac{1}{\mu}\|\nabla \mathcal{L}(\mathbf{w})\|_*^2 + \frac{1}{2\mu}\|\nabla \mathcal{L}(\mathbf{w})\|_*^2 \quad (48)$$

$$1169 \quad = \mathcal{L}(\mathbf{w}) - \frac{1}{2\mu}\|\nabla \mathcal{L}(\mathbf{w})\|_*^2, \quad (49)$$

1171 so

$$1172 \quad \|\nabla \mathcal{L}(\mathbf{w})\|_*^2 \geq 2\mu(\mathcal{L}(\mathbf{w}) - \mathcal{L}_*), \quad (50)$$

1174 which is the PL property we need.

1175 Lemma E.3 implies that \mathcal{L} is L -smooth with $L = S$, so

$$1177 \quad \mathcal{L}(\mathbf{w}_{t+1}) \leq \mathcal{L}(\mathbf{w}_t) + \langle \nabla \mathcal{L}(\mathbf{w}_t), \mathbf{w}_{t+1} - \mathbf{w}_t \rangle + \frac{S}{2}\|\mathbf{w}_{t+1} - \mathbf{w}_t\|^2 \quad (51)$$

$$1179 \quad \leq \mathcal{L}(\mathbf{w}_t) + \eta\|\nabla \mathcal{L}(\mathbf{w}_t)\|_* \langle \nabla \mathcal{L}(\mathbf{w}_t), (\nabla \mathcal{L}(\mathbf{w}_t))_* \rangle + \frac{S\eta^2\|\nabla \mathcal{L}(\mathbf{w}_t)\|_*^2}{2} \|(\nabla \mathcal{L}(\mathbf{w}_t))_*\|^2 \quad (52)$$

$$1182 \quad \leq \mathcal{L}(\mathbf{w}_t) - \eta\|\nabla \mathcal{L}(\mathbf{w}_t)\|_*^2 + \frac{S\eta^2\|\nabla \mathcal{L}(\mathbf{w}_t)\|_*^2}{2} \quad (53)$$

$$1184 \quad \leq \mathcal{L}(\mathbf{w}_t) - \eta \left(1 - \frac{\eta S}{2} \right) \|\nabla \mathcal{L}(\mathbf{w}_t)\|_*^2 \quad (54)$$

$$1186 \quad \leq \mathcal{L}(\mathbf{w}_t) - 2\mu\eta \left(1 - \frac{\eta S}{2} \right) (\mathcal{L}(\mathbf{w}_t) - \mathcal{L}_*), \quad (55)$$

1188 where the last line uses the PL property from (50) and that $\eta < 2/S$. Subtracting \mathcal{L}_* from both
 1189 sides:

$$1190 \quad 1191 \quad \mathcal{L}(\mathbf{w}_{t+1}) - \mathcal{L}_* \leq \left(1 - 2\mu\eta \left(1 - \frac{\eta S}{2}\right)\right) (\mathcal{L}(\mathbf{w}_t) - \mathcal{L}_*), \quad (56)$$

1192 so that for all t ,

$$1193 \quad 1194 \quad \mathcal{L}(\mathbf{w}_t) - \mathcal{L}_* \leq \left(1 - 2\mu\eta \left(1 - \frac{\eta S}{2}\right)\right)^t (\mathcal{L}(\mathbf{w}_0) - \mathcal{L}_*). \quad (57)$$

□

1197 The key to showing divergence when $\eta > 2/S$ (Theorem 5.2) is the following lemma.

1199 **Lemma 5.3.** If $\hat{\mathbf{d}} \in \arg \max_{\|\mathbf{d}\|=1} \mathbf{d}^\top \mathbf{H} \mathbf{d}$, then $(\mathbf{H} \hat{\mathbf{d}})_* = \hat{\mathbf{d}}$.

1202 *Proof.* Since \mathbf{H} is symmetric and PSD, we have for any such \mathbf{v}

$$1203 \quad (\mathbf{v} - \hat{\mathbf{w}})^\top \mathbf{H} (\mathbf{v} - \hat{\mathbf{w}}) \geq 0 \quad (58)$$

$$1204 \quad \mathbf{v}^\top \mathbf{H} \mathbf{v} - 2\mathbf{v}^\top \mathbf{H} \hat{\mathbf{w}} + \hat{\mathbf{w}}^\top \mathbf{H} \hat{\mathbf{w}} \geq 0 \quad (59)$$

$$1205 \quad \mathbf{v}^\top \mathbf{H} \mathbf{v} + \hat{\mathbf{w}}^\top \mathbf{H} \hat{\mathbf{w}} \geq 2\mathbf{v}^\top \mathbf{H} \hat{\mathbf{w}} \quad (60)$$

$$1206 \quad 2\hat{\mathbf{w}}^\top \mathbf{H} \hat{\mathbf{w}} \geq 2\mathbf{v}^\top \mathbf{H} \hat{\mathbf{w}} \quad (61)$$

$$1207 \quad \hat{\mathbf{w}}^\top \mathbf{H} \hat{\mathbf{w}} \geq \mathbf{v}^\top \mathbf{H} \hat{\mathbf{w}}, \quad (62)$$

1209 where the fourth line uses that $\hat{\mathbf{w}}^\top \mathbf{H} \hat{\mathbf{w}} \geq \mathbf{v}^\top \mathbf{H} \mathbf{v}$. Therefore

$$1210 \quad 1211 \quad (\mathbf{H} \hat{\mathbf{w}})_* = \underset{\|\mathbf{v}\|=1}{\operatorname{argmax}} \mathbf{v}^\top \mathbf{H} \hat{\mathbf{w}} = \hat{\mathbf{w}}. \quad (63)$$

□

1214 **Theorem 5.2.** Let $\mathcal{L}(\mathbf{w}) := \frac{1}{2} \mathbf{w}^\top \mathbf{H} \mathbf{w}$ for some $\mathbf{H} \succ 0$. For some norm $\|\cdot\|$, define the general-
 1215 ized sharpness $S := \max_{\|\mathbf{d}\| \leq 1} \mathbf{d}^\top \mathbf{H} \mathbf{d}$. If we run non-Euclidean GD (Def. 1.1) on \mathcal{L} , there exists
 1216 an initialization \mathbf{w}_0 from which GD will diverge for any step-size $\eta > 2/S$.

1217

1218 *Proof.* Let $\mathbf{w}_0 \in \operatorname{span}(\hat{\mathbf{d}})$ for some $\hat{\mathbf{d}} \in \arg \max_{\|\mathbf{d}\|=1} \mathbf{d}^\top \mathbf{H} \mathbf{d}$, so $\hat{\mathbf{d}} = \mathbf{w}_0 / \|\mathbf{w}_0\|$. We will show

1219 $\mathbf{w}_t = (1 - \eta S)^t \mathbf{w}_0$ by induction on t . With the property of $\hat{\mathbf{d}}$ from Lemma 5.3, the proof is
 1220 essentially a direct calculation. From the definition of gradient descent,

$$1223 \quad \mathbf{w}_{t+1} = \mathbf{w}_t - \eta \|\mathbf{H} \mathbf{w}_t\|_* (\mathbf{H} \mathbf{w}_t)_* \quad (64)$$

$$1224 \quad 1225 \quad = \|\mathbf{w}_0\| (1 - \eta S)^t \hat{\mathbf{d}} - \eta \|\mathbf{w}_0\| (1 - \eta S)^t \|\mathbf{H} \hat{\mathbf{d}}\|_* ((\|\mathbf{w}_0\| (1 - \eta S)^t \mathbf{H} \hat{\mathbf{d}})_* \quad (65)$$

$$1226 \quad 1227 \quad = \|\mathbf{w}_0\| (1 - \eta S)^t \hat{\mathbf{d}} - \eta \|\mathbf{w}_0\| (1 - \eta S)^t \|\mathbf{H} \hat{\mathbf{d}}\|_* (\mathbf{H} \hat{\mathbf{d}})_* \quad (66)$$

$$1228 \quad 1229 \quad = \|\mathbf{w}_0\| (1 - \eta S)^t \hat{\mathbf{d}} - \eta \|\mathbf{w}_0\| (1 - \eta S)^t \|\mathbf{H} \hat{\mathbf{d}}\|_* \hat{\mathbf{d}} \quad (67)$$

$$1230 \quad 1231 \quad = \|\mathbf{w}_0\| (1 - \eta S)^t \left(1 - \eta \|\mathbf{H} \hat{\mathbf{d}}\|_*\right) \hat{\mathbf{d}} \quad (68)$$

$$1232 \quad = \|\mathbf{w}_0\| (1 - \eta S)^{t+1} \hat{\mathbf{d}} \quad (69)$$

$$1233 \quad = (1 - \eta S)^{t+1} \mathbf{w}_0. \quad (70)$$

1234 where the second line uses the inductive hypothesis, the third line uses that the dual map $v \mapsto (v)_*$
 1235 is invariant to positive scaling of the input, uses Lemma 5.3, and the fifth line uses

$$1236 \quad 1237 \quad \|\mathbf{H} \hat{\mathbf{d}}\|_* = \sup_{\|\mathbf{v}\|=1} \mathbf{v}^\top \mathbf{H} \hat{\mathbf{d}} = (\mathbf{H} \hat{\mathbf{d}})_* \mathbf{H} \hat{\mathbf{d}} = \hat{\mathbf{d}}^\top \mathbf{H} \hat{\mathbf{d}} = \sup_{\|\mathbf{v}\|=1} \mathbf{v}^\top \mathbf{H} \mathbf{v} = S. \quad (71)$$

□

1239
 1240 As an aside, we can also show that GD will diverge for *every* initialization when η is sufficiently
 1241 large.

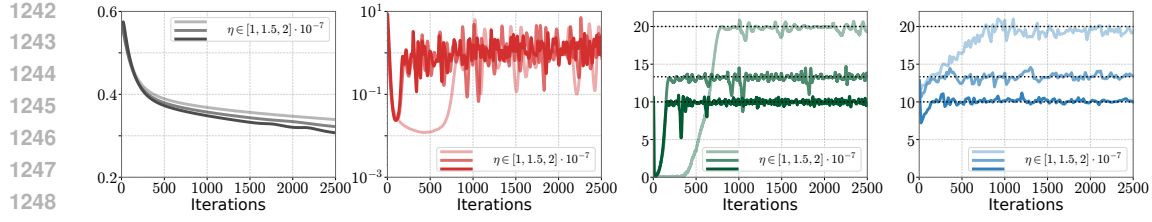


Figure F.1: (ℓ_∞ -descent) Train loss, gradient norm, directional smoothness, and generalized sharpness (14) during training CNN on CIFAR10-5k with ℓ_∞ -descent. Horizontal dashed lines correspond to the value $2/\eta$. Gradient norm and train loss curves are smoothed using an exponential smoothing with $\alpha = 0.1$. We use FW with $K = 50$ and $M = 5$ to approximate (14).

Theorem E.5. Let $\mathcal{L}(\mathbf{w}) := \frac{1}{2}\mathbf{w}^\top \mathbf{H}\mathbf{w}$ for some $\mathbf{H} \succ 0$. For some norm $\|\cdot\|$, define the generalized sharpness $S^{\|\cdot\|} := \max_{\|\mathbf{d}\| \leq 1} \mathbf{d}^\top \mathbf{H}\mathbf{d}$. Then, if we run non-Euclidean GD (Definition 1.1) on \mathcal{L} , there GD will diverge for every initial point \mathbf{w}_0 any step-size $\eta > 2/\mu$.

Proof. Starting from the definition of gradient descent,

$$\mathbf{w}_{t+1} = \mathbf{w}_t - \eta \|\mathbf{H}\mathbf{w}_t\|_* (\mathbf{H}\mathbf{w}_t)_* \quad (72)$$

$$\mathbf{H}\mathbf{w}_{t+1} = \mathbf{H}\mathbf{w}_t - \eta \|\mathbf{H}\mathbf{w}_t\|_* \mathbf{H}(\mathbf{H}\mathbf{w}_t)_* \quad (73)$$

$$\|\mathbf{H}\mathbf{w}_{t+1}\|_* = \left\| \mathbf{H}\mathbf{w}_t - \eta \|\mathbf{H}\mathbf{w}_t\|_* \mathbf{H}(\mathbf{H}\mathbf{w}_t)_* \right\|_* \quad (74)$$

$$\|\mathbf{H}\mathbf{w}_{t+1}\|_* \geq \eta \|\mathbf{H}\mathbf{w}_t\|_* \left\| \mathbf{H}(\mathbf{H}\mathbf{w}_t)_* \right\|_* - \|\mathbf{H}\mathbf{w}_t\|_* \quad (75)$$

$$\|\mathbf{H}\mathbf{w}_{t+1}\|_* \geq \left(\eta \left\| \mathbf{H}(\mathbf{H}\mathbf{w}_t)_* \right\|_* - 1 \right) \|\mathbf{H}\mathbf{w}_t\|_*. \quad (76)$$

We can bound the coefficient of η as

$$\left\| \mathbf{H}(\mathbf{H}\mathbf{w}_t)_* \right\|_* \geq \inf_{\|\mathbf{v}\|=1} \|\mathbf{H}\mathbf{v}\|_* = \inf_{\|\mathbf{v}\|=1} \sup_{\|\mathbf{u}\|=1} \mathbf{u}^\top \mathbf{H}\mathbf{v} \geq \inf_{\|\mathbf{v}\|=1} \mathbf{v}^\top \mathbf{H}\mathbf{v} = \mu, \quad (77)$$

so

$$\|\mathbf{H}\mathbf{w}_{t+1}\|_* \geq (\eta\mu - 1) \|\mathbf{H}\mathbf{w}_t\|_*, \quad (78)$$

and therefore

$$\|\mathbf{H}\mathbf{w}_t\|_* \geq (\eta\mu - 1)^t \|\mathbf{H}\mathbf{w}_0\|_*. \quad (79)$$

Since $\eta > 2/\mu \implies \eta\mu - 1 > 1$, the parameter norm $\|\mathbf{H}\mathbf{w}_t\|_*$ increases exponentially, and GD diverges. \square

F ADDITIONAL EXPERIMENTAL RESULTS WITH ℓ_∞ DESCENT

F.1 CONVERGENCE WHEN TRAINING CNN MODEL

F.2 SENSITIVITY OF FRANK-WOLFE ALGORITHM IN ESTIMATING THE GENERALIZED SHARPNESS FOR SIGN GRADIENT DESCENT

In this section, we study the sensitivity of the Frank-Wolfe algorithm in estimating the generalized sharpness of non-Euclidean gradient descent methods. Our experiments are conducted on a CNN with two convolutional layers, followed by a linear layer, trained on the CIFAR10-5k dataset (Krizhevsky & Hinton, 2009). We run ℓ_∞ -descent, and approximate the generalized sharpness by Frank-Wolfe with 50 iterations, using $\{1, 7, 15\}$ initialization points drawn from a standard normal distribution, and take the maximum over restarts as the generalized sharpness estimate.

In Fig. F.2, we show that the Frank-Wolfe estimate of the generalized sharpness is sensitive to the number of restarts. With a single random initialization, the algorithm generally underestimates the

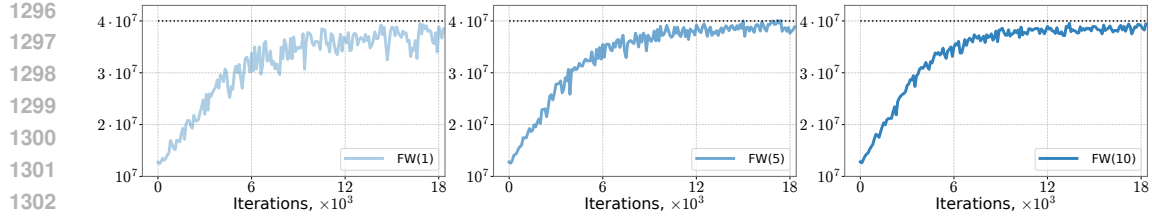


Figure F.2: The approximation of the generalized sharpness of ℓ_∞ -descent by the Frank-Wolfe algorithm varying the number of initialization points in $\{1, 5, 10\}$ for the Frank-Wolfe algorithm. Here, FW(k) denotes k restarts of the Frank-Wolfe algorithm, with varying initialization points.

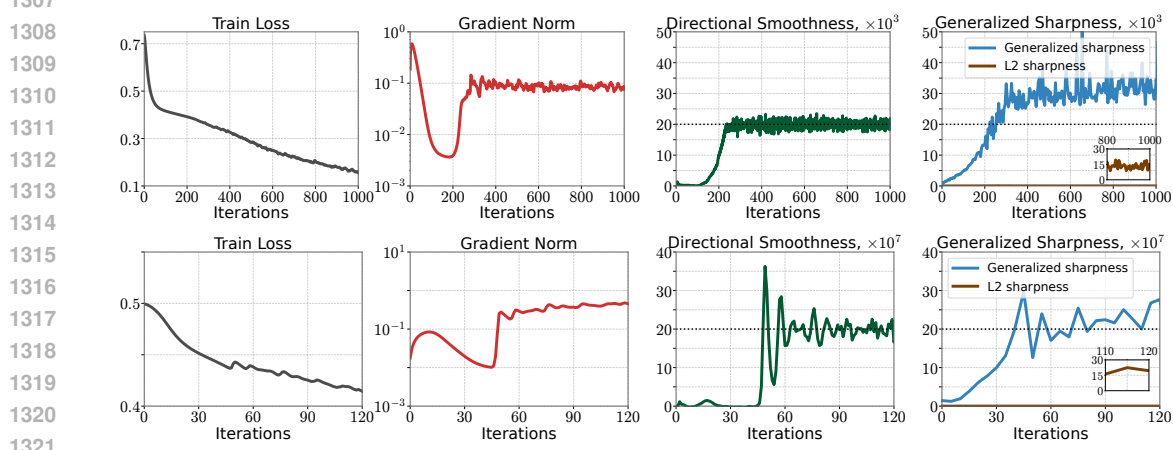


Figure F.3: (ℓ_∞ -descent) Train loss, gradient norm, directional smoothness, generalized sharpness (14), and L2 sharpness ($\lambda_{\max}(\nabla^2 \mathcal{L}(\mathbf{w}_t))$) during training Resnet20 (top, $\eta = 10^{-4}$) and VGG11 (bottom, $\eta = 10^{-7}$) on CIFAR10 with ℓ_∞ -descent. Horizontal dashed lines correspond to the value $2/\eta$.

value. Increasing the number of restarts to 15 yields a much more stable estimate that closely aligns with the true value almost everywhere.

F.3 RESULTS ON RESNET20 AND VGG11

In this section, we provide additional empirical results on larger models, such as Resnet20 (He et al., 2016) and VGG11 (Simonyan & Zisserman, 2014), trained on the CIFAR10 dataset with ℓ_∞ -descent and MSE loss. From the results in Figure H.5, we observe that both directional smoothness and generalized sharpness hover at the stability threshold $2/\eta$. In contrast, a standard notion of sharpness, i.e., $\lambda_{\max}(\nabla^2 \mathcal{L}(\mathbf{w}_t))$ defined in the Euclidean norm, lies significantly below the threshold (brown line in the right subfigure). Note that for Resnet20 model, the generalized sharpness stabilizes slightly above the threshold due to several unstable directions as explained in Section C.

G ADDITIONAL EXPERIMENTAL RESULTS WITH BLOCK GRADIENT DESCENT

G.1 TRAINING DETAILS

Our implementation is based on open source code from Cohen et al. (2021) together with publicly available datasets. In all our experiments, we use algorithms with full-batch gradient, i.e., we run them in the deterministic setting. The datasets and step-sizes η used in the experiments are specified in the figures. In not specified, we use the Frank-Wolfe algorithm with $M = 5$ restarts and $K = 50$ iterations, and PolarExpress with 5 steps.

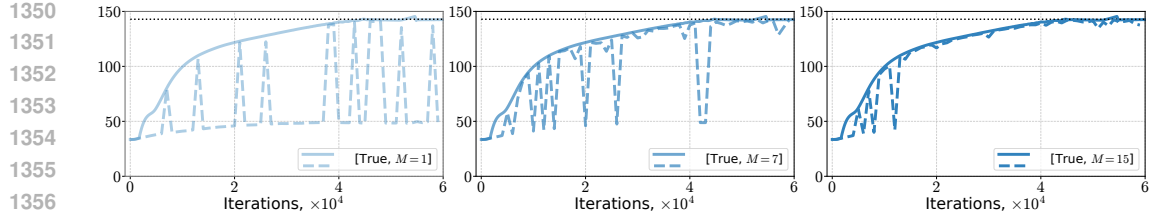


Figure G.1: The maximum block-wise Hessian eigenvalue (solid line), which is the generalized sharpness of Block CD, and its approximation by the Frank-Wolfe algorithm varying the number of initialization points in $\{1, 7, 15\}$ for the Frank-Wolfe algorithm. Here, M is the number of restarts of the Frank-Wolfe algorithm, varying the initialization point.

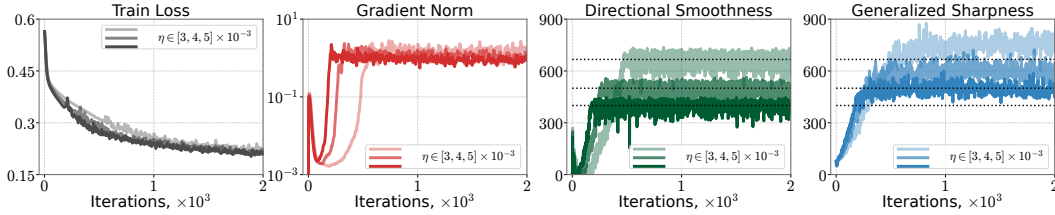


Figure H.1: (Spectral GD) Train loss, gradient norm, directional smoothness, and generalized sharpness (19) during training CNN model on CIFAR10 dataset with the Spectral GD. Horizontal dashed lines correspond to the value $2/\eta$.

In the training of CNN and MLP models, we use MSE loss, while in the training of the Transformer model, we use a rescaled MSE loss from [Hui & Belkin \(2020\)](#).

G.2 SENSITIVITY OF FRANK-WOLFE ALGORITHM IN ESTIMATING THE GENERALIZED SHARPNESS FOR BLOCK GRADIENT DESCENT

In this section, we study the sensitivity of the Frank-Wolfe algorithm in estimating the generalized sharpness of non-Euclidean gradient descent methods. Our experiments are conducted on a CNN with four convolutional layers, followed by a linear layer, trained on the CIFAR10-5k dataset ([Krizhevsky & Hinton, 2009](#)). Now we evaluate Block GD, where the generalized sharpness has a closed-form expression (30). We run Frank-Wolfe for 50 iterations, using $\{1, 7, 15\}$ initialization points drawn from a standard normal distribution, and take the maximum over restarts as the generalized sharpness estimate. The Frank-Wolfe procedure is applied every 100 iterations of Block CD.

In Fig. G.1, we show that the Frank-Wolfe estimate of the maximum block-wise Hessian eigenvalue is sensitive to the number of restarts. With a single random initialization, the algorithm provides a good approximation at a few iterations but generally underestimates the value. Increasing the number of restarts to 15 yields a much more stable estimate that closely aligns with the true value almost everywhere.

H ADDITIONAL EXPERIMENTAL RESULTS WITH SPECTRAL GRADIENT DESCENT

H.1 CONVERGENCE WHEN TRAINING CNN MODEL

In this section, we present the results when training CNN model on CIFAR10 dataset with Spectral GD; see Figure H.1. The results support our theoretical observations.

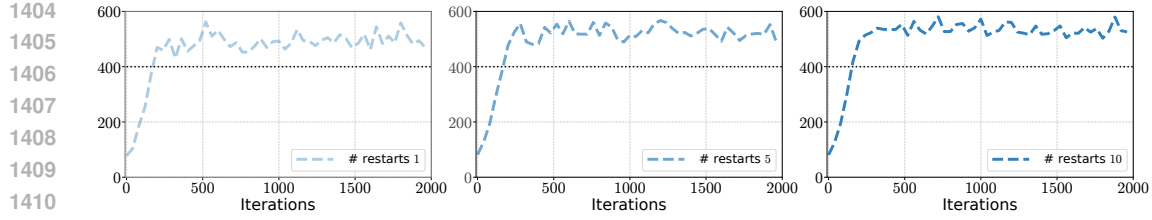


Figure H.2: The approximation of the generalized sharpness by the Frank-Wolfe algorithm for Spectral GD varying the number of initialization points in $\{1, 5, 10\}$ for the Frank-Wolfe algorithm.

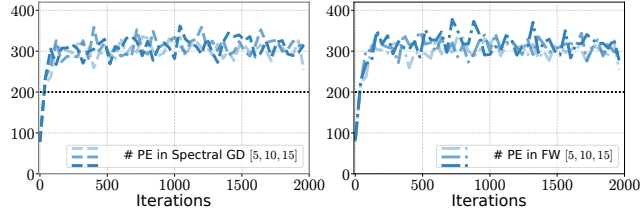


Figure H.3: The sensitivity of the generalized sharpness estimation of Spectral GD to the number of Polar Express steps in Spectral GD (left) and in Frank-Wolfe (right). Here $\# \text{ PE}$ means the number of Polar Express steps in Spectral GD or Frank-Wolfe algorithm respectively.

H.2 SENSITIVITY OF FRANK-WOLFE ALGORITHM IN ESTIMATING THE GENERALIZED SHARPNESS FOR SPECTRAL GRADIENT DESCENT

Next, we switch to the Spectral GD to train CNN model on the full CIFAR10 dataset. We perform a similar procedure to the one done in the previous section. We fix the number of Polar Express steps in both Spectral GD and Frank-Wolfe to 5 and vary the number of initialization points for Frank-Wolfe in $\{1, 5, 10\}$. Each run of Frank-Wolfe has 50 iterations.

In Fig. H.2, we observe that Spectral GD is less sensitive to the number of initialization points for Frank-Wolfe than Block GD. Therefore, it is not necessary to do restarts for Frank-Wolfe when it is used to measure the generalized sharpness of the Spectral GD algorithm.

H.3 SENSITIVITY OF SPECTRAL GRADIENT DESCENT TO THE NUMBER OF POLAR EXPRESS STEPS

We investigate how the number of Polar Express steps affects the generalized sharpness estimation of Spectral GD. To this end, we fix the number of Polar Express steps in Spectral GD and vary the number of steps in the Frank-Wolfe algorithm across $\{5, 10, 15\}$, and vice versa. All experiments are conducted using a CNN with four convolutional layers, trained on the full CIFAR-10 dataset.

As shown in Fig. H.3, we do not observe any significant differences across the different configurations. This indicates that 5 steps of the Polar Express algorithm are sufficient to obtain an accurate and stable estimate of Spectral GD’s generalized sharpness.

H.4 QUADRATIC TAYLOR APPROXIMATION OF THE REAL OBJECTIVE

H.5 RESULTS ON RESNET20 AND VGG11

In this section, we provide additional empirical results on larger models, including ResNet20 (He et al., 2016) and VGG11 (Simonyan & Zisserman, 2014), trained on the CIFAR10 dataset using Spectral GD with MSE loss. As shown in Figure H.5, both the directional smoothness and the generalized sharpness remain close to the stability threshold $2/\eta$. In contrast, the standard notion of sharpness—namely $\lambda_{\max}(\mathcal{L}(\mathbf{w}_t))$ computed in the Euclidean norm—stays well below this thresh-

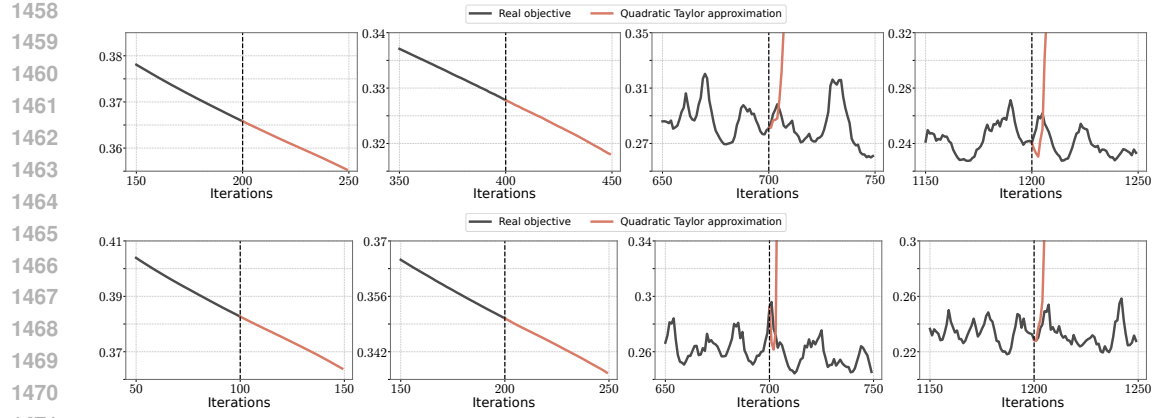


Figure H.4: MSE loss (top row $\eta = 0.003$, bottom row $\eta = 0.004$). At 4 different iterations during the training of the CNN from Fig. 4 (marked by the vertical dotted black lines), we switch from running Spectral GD on the real neural training objective (for which the train loss is plotted in gray) to running Spectral GD on the quadratic Taylor approximation around the current iterate (for which the train loss is plotted in orange). Two left figures are timesteps before Spectral GD has entered EoS; observe that the orange line (Taylor approximation) closely tracks the blue line (real objective). Two right figures are timesteps during the EoS; observe that the orange line quickly diverges, whereas the blue line does not.

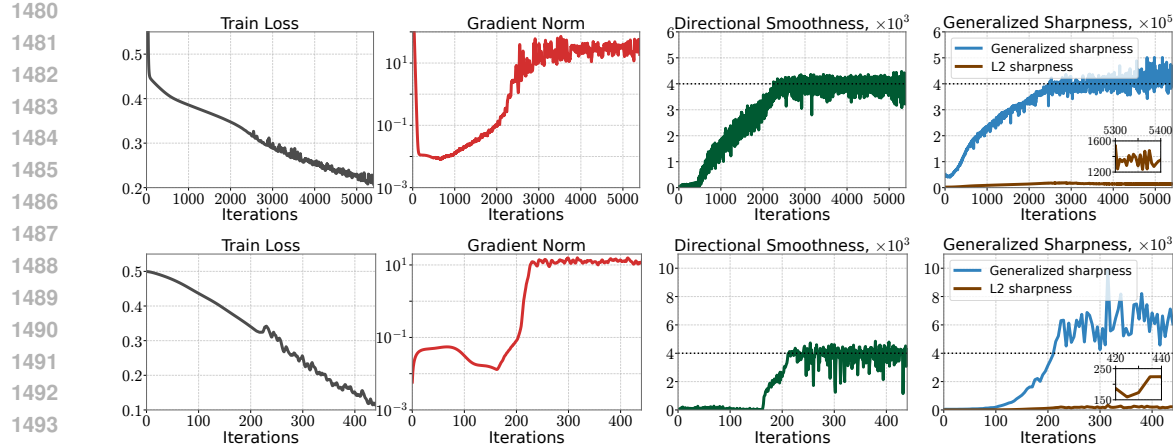


Figure H.5: (Spectral GD) Train loss, gradient norm, directional smoothness, generalized sharpness (14), and L2 sharpness ($\lambda_{\max}(\nabla^2 \mathcal{L}(\mathbf{w}_t))$) during training Resnet20 (top, $\eta = 5 \cdot 10^{-5}$) and VGG11 (bottom, $\eta = 5 \cdot 10^{-4}$) on CIFAR10 with ℓ_∞ -descent. Horizontal dashed lines correspond to the value $2/\eta$.

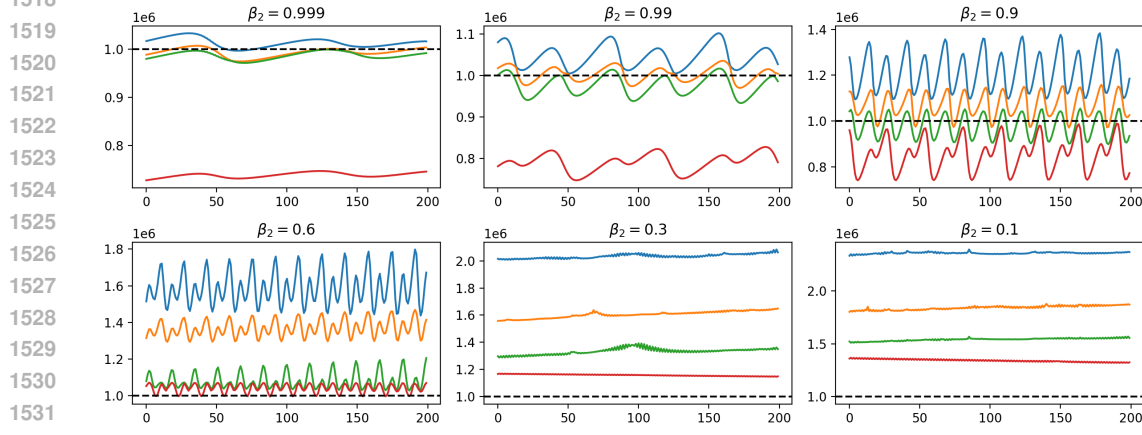
old (brown curve in the right panel). For the ResNet20 model, the generalized sharpness stabilizes slightly above $2/\eta$, which can be attributed to the presence of several unstable directions, as discussed in Section C.

I ℓ_∞ -DESCENT AND RMSPROP

In this section, we report results for the RMSprop algorithm when training an MLP on the CIFAR10-5k subset with MSE loss. Although SignGD can be viewed as a limiting case of RMSprop as $\beta_2 \rightarrow 0$, the adaptive EoS (AEoS) condition of Cohen et al. (2022) is valid only when β_2 is large (i.e., close to 1 in practical settings) and breaks down as β_2 becomes small. For small β_2 , the largest eigenvalue of the preconditioned Hessian $\lambda_{\max}(P_t^{-1} \nabla^2 \mathcal{L}(\mathbf{w}_t))$ does not stabilize around $2/\eta$; instead, it often exceeds this value by a substantial margin. The underlying issue is that as $\beta_2 \rightarrow 0$, the algorithm no

1512 longer resembles preconditioned gradient descent with a slowly-changing preconditioner, which is
 1513 the approximation that inspires the AEoS condition.
 1514

1515 Our results in Figure I.1 support this observation. We plot the top four eigenvalues of the precondi-
 1516 tioned Hessian for RMSprop, showing that they stabilize around the threshold $2/\eta$ only when β_2 is
 1517 large, while for small β_2 the behavior deviates significantly.
 1518



1533 Figure I.1: Sharpness of RMSprop when training MLP model on a subset of CIFAR10 dataset,
 1534 varying β_2 hyperparameter. Here, colored lines correspond to the evolution of the top-4 largest
 1535 eigenvalues of the preconditioned Hessian, while the dashed line is $2/\eta$ threshold. We observe that
 1536 RMSprop reaches AEoS only for realistic (close to 1) values of β_2 , while for small β_2 the precondi-
 1537 tioned sharpness is not at $2/\eta$, but significantly higher.
 1538
 1539
 1540
 1541
 1542
 1543
 1544
 1545
 1546
 1547
 1548
 1549
 1550
 1551
 1552
 1553
 1554
 1555
 1556
 1557
 1558
 1559
 1560
 1561
 1562
 1563
 1564
 1565